This is to certify that the

thesis entitled

Stamping Analysis of Textile Composite Preforms

presented by

Ran Mohan Jit Singh Sidhu

has been accepted towards fulfillment
of the requirements for

Master of Science degree in Dept. of Materials Science and Mechanics

Ronald C. Averill

Major professor

Date 12/8/00

STAMPING ANALYSIS OF TEXTILE COMPOSITE PREFORMS

By

Ran Mohan Jit Singh Sidhu

A THESIS

Submitted to
Michigan State University
in partial fulfillment of the requirements
for the degree of

MASTER OF SCIENCE

Department of Materials Science and Mechanics

2000

ABSTRACT

STAMPING ANALYSIS OF TEXTILE COMPOSITE PREFORMS

By

Ran Mohan Jit Singh Sidhu

A finite element model has been developed for the stamping analysis of plain weave textile composite preforms. This model is simple, efficient and can be used with existing finite element codes. The model represents the preform as a mesh of 3-D truss elements and 3-D shell elements. The tows are modeled explicitly through the truss elements. Inter tow sliding has been taken into account in the model. The shell elements represent a fictitious material, which we called the transforming medium that models the effects of inter tow friction and fiber angle jamming. The model takes into account large strains and large deformations. In-plane uni-axial tension tests were performed on plain weave specimens for determining the constitutive law of the transforming medium. Use of the model is demonstrated by simulating the stamping of a preform over a sphere. The results from the simulation show good correlation with the results from the experiments.

Dedicated to my Grandparents and Parents

ACKNOWLEDGMENTS

I would like to thank my advisor Dr. Averill for his incredible guidance, expertise and foresight throughout the research. I would also like to thanks Dr. Pourboghrat for his support and advice and Sakeb for his hard work and assistance with the experimental work. I would also like to thank the MSM faculty for the immense knowledge that I gained through the courses.

Furthermore I would like to thank my family for all their support and guidance throughout the period of my research.

TABLE OF CONTENTS

List of Figures

List of Tables

Chapter 1

1 INTRODUCTION

1.1 Introduction

The importance of fabric reinforced composites hardly needs to be emphasized. They have a variety of applications in various industries, especially as structural components in the automobile, aerospace, marine, infrastructure and recreation industries. The main advantage of using these materials is their high specific strength. In the past these fabric reinforced composites were manufactured by laying up the yarn bundles in the mold directly before injecting the resin. However, this process of manufacturing was very labor intensive and also very cost inefficient. The manufacture of these composites has been made more efficient by weaving yarn bundles into a fabric sheet and then forming this preform to the shape of the desired object prior to introducing a matrix material.

It is known that bending, stretching, and shearing of textile preforms affects the orientation, the cross-sectional shape, the crimp angle, and the density of tows in the preform. As a result, draping or forming of preforms may result in large changes in the microstructure of the preform. These changes in turn strongly affect the permeability of the preform as well as the local stiffness and strength of the ensuing composite. Deleterious microstructural distortion is usually most severe near regions of high spatial curvature, making these already

critical structural regions even more prone to premature failure. Prediction of failure in these regions cannot be based on nominal properties of flat coupon specimens. Rather, some estimate of the local stiffness and strength (both dependent on the microstructure and the processing conditions) must be known in order to provide a reasonable estimate of structural failure loads. Also, the evolved microstructure after deformation is important for the permeability calculations for modeling mold filling processes. The evolution of the orientation of the tows of the preform during the deformation process thus needs to be accurately determined in order to determine these properties of the deformed preform.

Also it is necessary to know if the preform being considered can be deformed onto the desired shape without wrinkling, and if the fiber orientation is unique or is sensitive to the method of forming as the formability of the fabric is greatly dependent on its architecture. The prediction of the microstructural evolution of the preform undergoing draping will result in a large saving in terms of time and money required in the designing of a die, without knowing if it will yield the desired results. If the preform does not deform to the shape of the die without wrinkling, the die is useless. This requires a simple finite element model, which can be used to simulate the draping process and predict accurately the deformed microstructure of the preform. A new finite element model has been proposed for the stamping analysis of a plain weave textile composite preform. This model is simple, efficient and can be used with existing finite element codes. The model represents the preform as a mesh of 3-D truss elements and 3-D shell

elements. The truss elements model the tows in the preform and are practically inextensible during the deformations resulting from the draping or stretch forming of the preforms. The truss elements are not pinned at the points of intersection, which allows for the modeling of sliding between the tows. The truss elements, representing the tows, are connected to each other, indirectly, through the shell elements. The shell elements represent a fictitious material, called the transition medium. This transition medium has a non-linear orthotropic material behavior and represents the effects of inter tow friction and the fiber angle jamming in the model. The model takes into account large strains and large deformations. In-plane uni-axial tension tests have been performed on plain weave preform specimens. These tests were used to determine the constitutive law of the transition medium and also to show that the inter fiber sliding in the preform is significant during even moderate strains on the overall preform. Use of the model is demonstrated by simulating the stamping of a preform over a sphere. The results from the simulation show good correlation with the results from the experiments.

1.2 Literature review

Several different approaches have been used to model the deformation behavior of the preform accurately but they fail to take into account all the aspects of the deformation behavior of the preform. Some of these techniques have been discussed below.

1.2.1 Dry Preforms

Robertson et al.[1,6] use the fisherman's net analogy for the computation of the evolution of the tow orientation. The tows are assumed to be inextensible and pinned at the inter-sections. They assume that the only available mode of deformation is the in-plane fiber shear. The position of each node (the point of inter-section of the tows) is found by solving the equations of the intersection of the weft and warp tow segments and the surface. So starting at the top the fabric is laid on the hemisphere one node at a time until the bottom edge is reached and then they can predict if wrinkling occurs. The ignoring of the fiber angle jamming and the pinned fibers lead to over prediction of fiber angles in the areas of high deformation.

Advani et al.[3-4] and Rudd et al.[5] used the fishnet technique to model the preform behavior. The fabric is replaced by an in-extensible net that allows only shearing of the fibers. As in the above models the inter-tow slippage has been ignored. However the jamming is implemented in their code. The information from this code is then used to calculate the fiber volume fractions and finally the permeability calculations.

Boisse et al.[7-8] represented the overall mechanical behavior of the fabric by combining the tensile behavior of a single thread and the position of the tows at that instant. The fabric is modeled using 3 and 4 noded membrane elements due to the low bending stiffness. They have modeled the complete tensile behavior of the tow including the undulation effect and the damage of the fibers obtained from the uni-axial and bi-axial tensile tests. Again in this model it has

been assumed that there is no sliding between the tows and the jamming has also been ignored.

McBride et al.[9-10] consider the entire architecture of the tows in modeling the mechanical behavior of the preforms. They identified the unit cell and described its configuration by a set of four cosinusoids. The geometry of the unit cell was formulated as a function of the fabric thickness, the yarn width, the yarn spacing and the yarn angle. The fabric thickness and the yarn spacing have been assumed to be independent of the yarn angle but the yarn width has been defined as a function of the yarn angle. So knowing the yarn angle the geometry of the fabric can be found. They use this formulation in combination with the fishnet model used in [1] to give the orientation and the geometry of the fabric with deformation.

Ascough[11] et al. used a beam element large displacement model for the simulation of fabric draping behavior. The fabric in this study is a cloth fabric with a much finer weave than that of the structural material preforms being considered here. In this model, the bending behavior of the cloth is governed by the stiffness properties of the beam elements. The fibers were not modeled explicitly. The goal was to predict the overall shape of the draped cloth rather than investigate the position or orientation of the fibers in the cloth. The beam elements used have mass and stiffness properties corresponding to a cloth width equivalent to the element pitch. Large displacement behavior is included. A Newmark time stepping approach is used for the analysis. The results compare well with the experiments, but a refined mesh requires high computational time.

1.2.2 Soft Matrix Fiber Reinforced Composites

All the above techniques have been used for the modeling of preforms. There are some other techniques, which have been used for the modeling of reinforced composite fabrics. Mauget et al.[12] used the laminate analogy to predict the fiber orientation of a soft composite structure. Since here the stiffness of the resin is very small as compared to the fibers it is very similar to a preform. They again assume the fibers to be pinned at the intersections and inextensible so the deformation of the fabric is represented as a change in the aspect ratio of the unit cell. The composite is modeled by thick shell elements or brick elements. The laminate theory is used to calculate the properties of the elements. The Poisson's ratio of the elements is updated with the change in the aspect ratio of the elements. The fiber angle reaches five degrees before jamming, which is less than the actual jamming angle for typical preforms.

Cherouat et al.[13,14] used a bi-component element to model reinforced composite preforms. They accounted for the non-linear behavior of the tows by taking into account the undulation effect of the tows. This renders a very small initial stiffness in the tows, as the initial force is used to straighten out the fibers. The resin is modeled as a visco-elastic material. Tow jamming and tow sliding have been ignored in the formulation.

1.3 Current model

Nearly all the approaches to date ignore the inter tow sliding, and the inter fiber jamming has not been modeled effectively in a few places where it has been considered. Another aspect that is missing in all the above approaches is the modeling of fabric imperfections. During the manufacturing process the tows are not aligned perfectly and there may be a lot of waviness in the tows. This is particularly the case in the tri-axially braided preforms where the axial tow is not straight. In our approach the tows are modeled explicitly and therefore the imperfections in the specimen can be modeled exactly as they are.

In the present paper a new model is developed to study the mechanical behavior of textile preforms. The aim of this study is to represent accurately the deformation behavior of a preform using a model that is simple to build. The unit cell of the preform is identified and is discretized with 2 noded 3-D truss elements and 4 noded 3-D shell elements. The truss elements are used to model the tows and the shell elements have been used to model the fictitious material (the air gaps between the tows), which we call the transition medium. The constitutive law of the fictitious material is characterized through uni-axial tensile tests on the specimen.

Chapter 2

2 THE PREFORM MODEL

2.1 Objectives

The main objective of this study was to develop a model for representing a textile preform undergoing an arbitrary shape change due to stretching or die forming, with the ability to accurately represent the microstructural evolution. The model should incorporate all the different modes of deformation during the draping or stretch forming of the preform. Another feature desired in the model was that it should lend itself for analysis using existing commercial finite element codes and should be simple to build. With all these desired features laid down the various modes of deformation taking place during the preform draping were identified. Figure 1 shows the general scheme of the tow layout in a plain weave preform.

2.2 Deformation Modes

The different modes of deformation of a woven or braided preform are tow straightening due to the undulations, fiber angle change due to scissoring of the tows, and inter tow sliding. These are discussed individually below.

The morphology of the plain weave composite preforms is such that the braider tows go over and under each other to form the entire preform. As a result, the tows in the plain weave composite preform are not straight, but, have a

curvature associated with them. This undulating curvature of the tows can be compared to a sine wave with a very small amplitude. This is shown in Figure 2. There are a few existing models that represent the tows as a sinusoidal curve, which is a function of the fabric geometry, and the fiber angle.

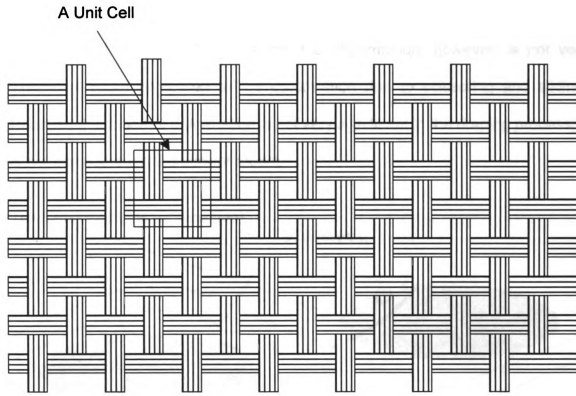

Figure 1. A simple representation of a plain weave preform. The square drawn on the preform represents one unit cell.

Due to this waviness associated with the tows, when a tensile load is applied to the preform the tows tend to straighten out the undulations first. The initial deformation, therefore, is not due to the elongation of the fibers but just to the fiber bundle straightening. The transverse shear stiffness of the tows in the

preform is very small as it is just a bundle of dry fibers. The low value of the transverse shear stiffness and a very small moment of inertia result in a very low bending stiffness of the tows. Thus, the initial stiffness is very low until the tows are nearly straightened or until they cannot straighten any further due to interaction between the tows, after which the stiffness is almost equal to that of the fibers. This mode of deformation does not affect the orientation of the tows or the shape of the fabric [8]. This mode of deformation, however, is not very significant when compared to the deformation due to scissoring and sliding. Because this mode of deformation is not very significant in the draping process, it is not considered in the current model.

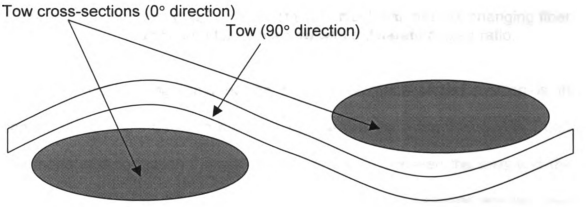

Figure 2. Undulation of a tow as it goes over one tow and then under the next tow.

The second mode of deformation in the plain weave preform is due to the scissoring of the tows. This is the primary mode of deformation in the preforms. This mode leads to the most significant changes in the microstructure of the preform. The scissoring refers to the change in the inter tow angle without any

change in the length of the tows. This can be described as the change in the aspect ratio of a rectangle, which has the tows as its diagonals. The length of these diagonals remains constant. This is depicted in Figure 3.

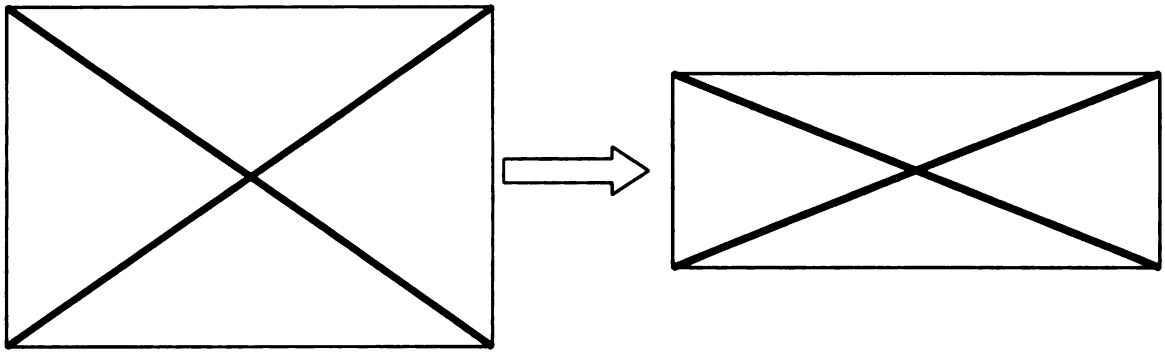

Figure 3. Scissoring deformation of the unit cell with the tow changing fiber angle and forming a bow with a different aspect ratio.

The only change that occurs during this mode of deformation is the change in the angle between the tows, i.e. the change in the fiber angle. During this mode of deformation there is no relative motion between the tows and they basically act as being pinned at the point of intersection between any two tows. This mode accounts for most of the deformation of the preform. The friction between the tows produces a resistance to the rotation of the tows about the point of intersection thereby producing a resistance to the deformation of the preform. The magnitude of this frictional resistance is very small and is assumed here to remain constant. This fact makes the scissoring mode the most predominant mode of deformation in the preform as the deformation will follow the path of least resistance to minimize energy. The effect of friction between the

tows has been modeled in the current model, even though the friction has not been modeled directly as friction between the tows. The details about the method and approach used to model the effect of friction and the deformation behavior have been dealt with in the sections to follow.

Unloading of the preform has not been considered in this model. The current model is only valid for the loading of the preform and does not truly capture the deformation behavior during the unloading of the preform. Energy is lost in the preform due to work done against friction during scissoring and sliding between the tows. Since this process is irreversible, this energy cannot be recovered. As a result, the actual preform will not follow the same stress-strain curve during unloading as it does during the loading and this has not been accounted for in this model.

As mentioned earlier, during the scissoring deformation of the preform the fiber angle changes. It has been shown experimentally that the fiber angle between the tows does not reach zero degrees with progressively increasing deformation of the fabric. There is a limit to the fiber angle to which the fabric can be sheared. As the preform is subjected to an increasing tensile strain, the tows scissor to a smaller fiber angle to accommodate the deformation of the fabric. Due to this the fiber angle keeps decreasing progressively, with increasing overall fabric tensile strain. As the fiber angle gets smaller it reaches a point where the spacing between the tows vanishes, i.e. the adjacent tows are in contact with each other at this point. This is shown in Figures 4 and 5. Figure 4 shows a part of four tows in the undeformed position with the angle between

them equal to the initial fiber angle of the preform. Figure 5 then shows the tows in the position where they just come in contact and the angle between the tows at this instant is the angle at which the stiffening behavior starts. This fiber angle is called the initial jamming angle, θ_{IJ} and is defined as the fiber angle at the point in time when the adjacent parallel tows come in contact with each other.

After reaching this angle, any further scissoring deformation takes place with the change in the width of the tows, as they are pressed closer together with the increasing tensile force on the preform.

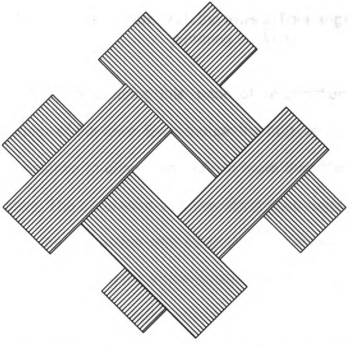

Figure 4. Part of four tows, which form a unit cell. The spacing between the tows is magnified in this figure.

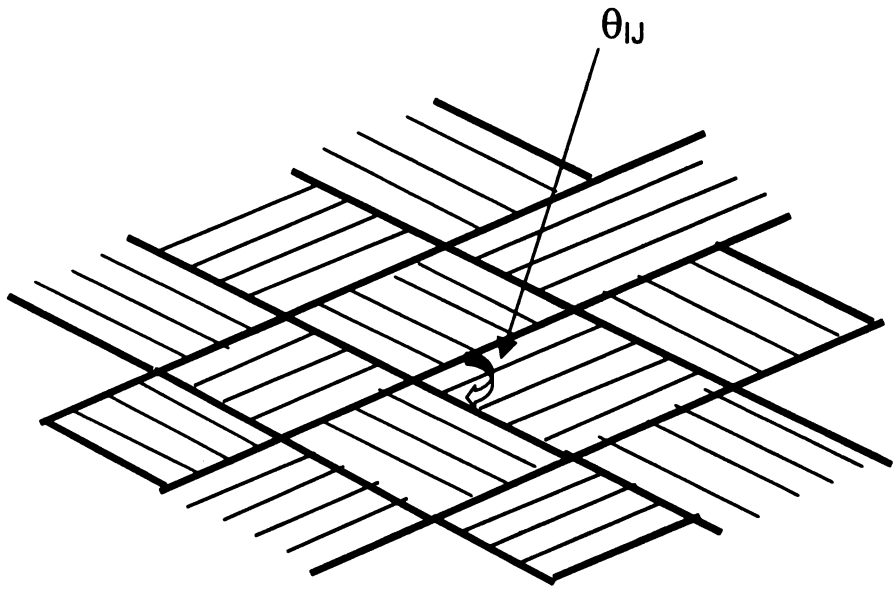

Figure 5. A part of the preform with the tows at fiber angle equal to the initial jamming angle, θ_{IJ}.

The initial stiffness during this mode of deformation depends upon the transverse stiffness of the tows. Even though the transverse stiffness of the tows is small, the resistance to change in width is more than the frictional resistance between the tows. The transverse stiffness of the tows increases with decreasing tow width due to the interaction with other tows. Moreover, since the tow width cannot decrease to zero there is a limit to the final fiber angle to which the fabric can shear. After reaching this angle no more shear deformation can occur. As a result, the stiffness to the shear deformation between the tows increases until it reaches this limiting shear angle, which is called the final fiber jamming angle. The value of this angle depends upon the type of weave, tightness of the tows (i.e., the tow spacing) and the original angle between the tows, which normally ranges from 15° to 20°. These values are half fiber angles, where half fiber angle

is defined as half of the fiber angle between the tows at that point. So after reaching this angle the fabric cannot deform any further by changing the fiber angle between the tows. In the current model the jamming has been incorporated through the constitutive law of the transition medium, which has been modeled by 3-D shell elements. The modeling and the material laws of the model are explained in the next section.

After reaching the jamming angle, the only possible mode of deformation that the tows can undergo to accommodate the tensile strain being applied to the fabric is the inter tow sliding, as the fiber angle between the tows cannot change any further. The sliding deformation of the tows is illustrated in Figure 6 below.

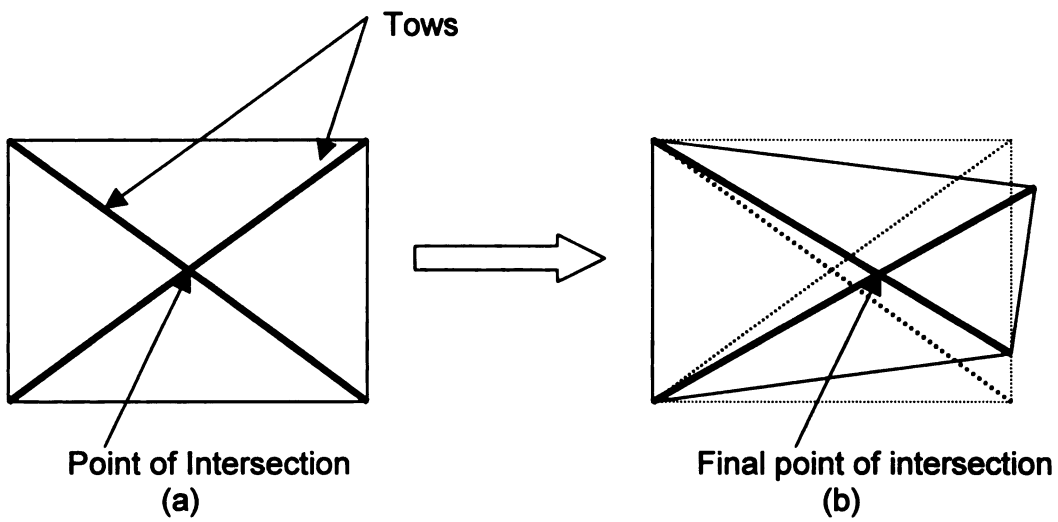

Figure 6. Sliding deformation in a unit cell. (a) The initial configuration. (b) The initial position and the final position of the tows after deformation. The point of intersection can be seen to have displaced.

This mode of deformation is significant in stamping processes involving large deformations. This aspect of deformation has been neglected in most other models proposed in this field as being insignificant. But as mentioned earlier this mode becomes significant during large deformations and henceforth cannot be

neglected. The sliding deformation has been accommodated through the connectivity of the elements and is controlled in the current model through the transition medium. The next section explains the unit cell and how all these modes of deformation have been incorporated through the constitutive law of the transition medium.

2.3 Calculation of the Jamming Angle

As discussed earlier the stiffening behavior of the preform starts when the adjacent tows come in contact with each other. At this point the force required to deform the preform increases as deformation now involves the change in the width of the tows in addition to the friction between the tows against scissoring and sliding. This is modeled by stiffening the shell elements when the fiber angle becomes equal to the initial jamming.

The jamming angle of the fabric is calculated from the geometry of the fabric. The theory and the equations used in this calculation have been taken from McBride and Chen's geometric model of the unit cell for plain weave fabrics. The geometry of the tows is modeled using a set of four sinusoidal curves. The width of the tows can be expressed as a function of the initial fabric geometry and the fiber angle. It has been shown by experiments that the fabric thickness is independent of the fiber angle [9]. For the present purpose, the fibers have been assumed to be pinned at the intersection of the tows. These equations are used in the current model for the calculation of the initial jamming angle, which marks the start of the stiffening behavior of the preform. Until this point the tows behave

basically as pinned thereby the assumption that the tows are pinned at the point of intersection is valid for these particular calculations. This is shown later in the experiments also validating the assumption as there is practically no sliding in the center portion of the preform specimen, where the fiber jamming occurs. The equation relating the tow width to the trellis angle is given below.

$$w(\theta) = w_0/(\sin\theta)^{(s_o - w_o)/\beta_o} \quad (1)$$

where w = is the tow width at fiber angle θ

w_0 = is the initial tow width at $\theta = 90°$

θ = is the fiber angle

s_o = is the tow spacing which remains constant

β_o = half period of sinusoid describing yarn cross-section at $\theta = 90°$

$$\beta_o = \pi w_o/(2\arccos[\sin^2(\pi w_o/4s_o)])$$

The criterion that has been used for the calculation of the initial jamming angle is that the stiffening behavior of the preform starts as soon as the adjacent tows come in contact with each other, i.e. when the when the gap between two adjacent tows in the preform is zero. This has been shown earlier in Figure 5. Using this criterion the initial fiber jamming angle is calculated in terms of the initial fabric geometry and the initial fiber angle.

Figure 7 shows the tows at the point when they just come in contact with each other and the associated dimensional details. Figure 8 shows the exploded view of the triangle ABC from the Figure 7.

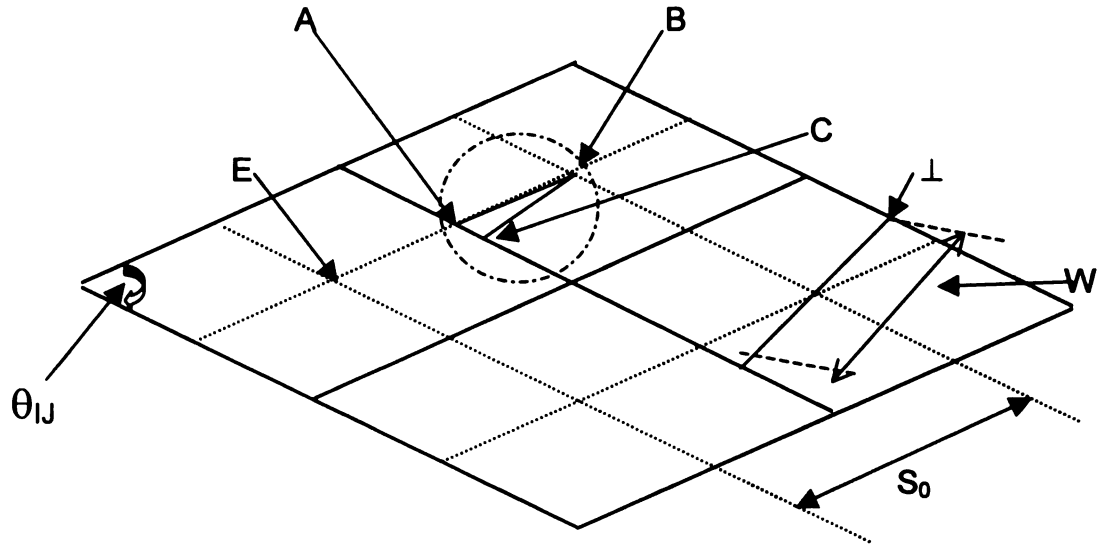

Figure 7. A part of 4 tows at a fiber angle equal to the initial fiber jamming angle. W in the figure is the tow width at this fiber angle and is the perpendicular distance between the boundary lines of the tow.

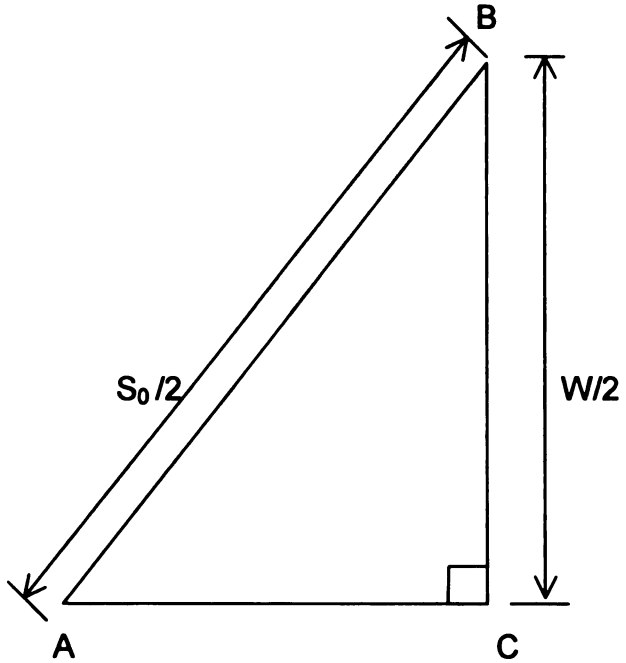

Figure 8. The exploded view of the triangle ABC from Figure 7.

Using the geometry of the tows as shown in the figures above and using simple trigonometric laws, a relation between the tow width w, the initial fiber jamming angle θ_{iJ}, and the initial tow spacing s_o can be formulated. The distance EB in Figure 9 is equal to the initial spacing between the tows, s_o , because of the assumption that the tows behave as pinned with no inter fiber sliding until this point. From triangle ABC

$$Sin\theta_{iJ} = \frac{w/2}{s_0/2} = \frac{w}{s_0} \qquad (2)$$

In Equation (2) above, w is given by the Equation (1). Substituting the value for w from Equation (1) into Equation (2) and solving for Sin θ_{iJ} :

$$Sin\theta_{iJ} = \left(\frac{w_0}{s_0}\right)^{\left(\frac{\beta_0}{\beta_0+s_0-w_0}\right)}$$

Finally, θ_{iJ} is given by :

$$\theta_{iJ} = ArcSin[(w_0 / s_0)^{\frac{\beta_0}{\beta_0+s_0-w_0}}]$$

where θ_{iJ} = is the initial fiber jamming angle.

The fiber angle calculated using the above equation is used to calculate the local unit cell normal strain at this point, which is then used in the material model to mark the start of the stiffening behavior. This strain calculation is again based on the assumption that the local tow deformation in the preform is mainly due to scissoring and that the tows behave as pin jointed members until that point. This way the unit cell can be represented as a rectangular box with the tows as the diagonals and the angle between the diagonals equal to the fiber

angle between the tows at that point. Since the length of the tows does not change during the scissoring deformation the change in the unit cell can be regarded as just a change in the aspect ratio of the rectangular box. This is shown in Figure 9.

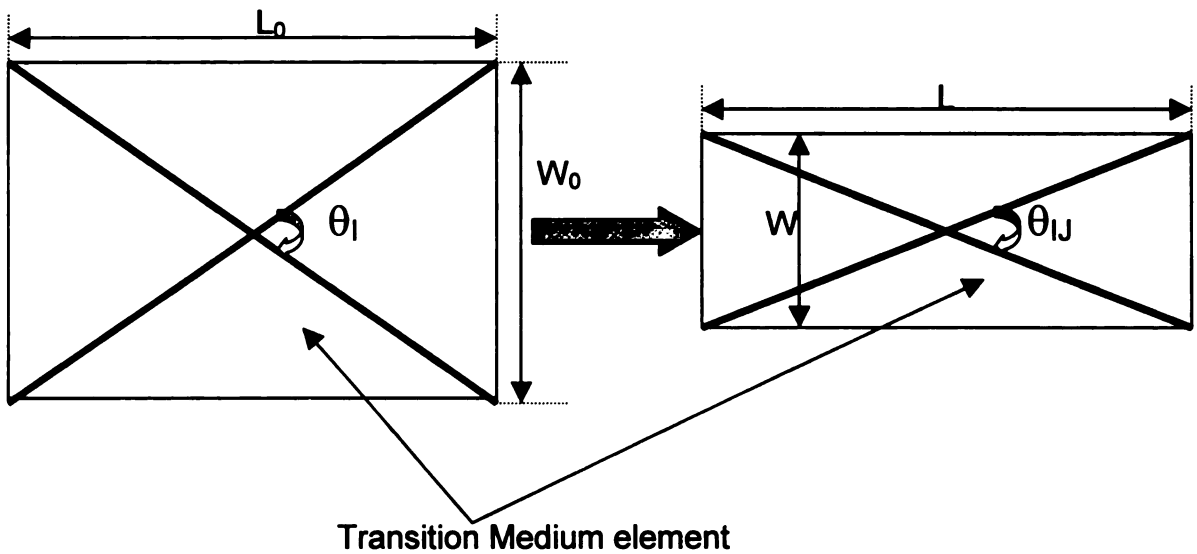

Figure 9. Scissoring from initial fiber angle to the initial jamming angle with the corresponding dimensions of the shell element.

Using the above figure the axial and the transverse strains can be calculated using the standard formula.

Normal strain at point of stiffening, ε_x and ε_y are given by

$$\varepsilon_x = \frac{L - L_0}{L_0}$$

$$\varepsilon_y = \frac{W - W_0}{W_0}$$

The final jamming angle is found from the experimental data.

2.4 Unit Cell

Various models were tried before finally settling on the current model. The description of all these models with their pros and cons are discussed in detail in the following section.

The main characteristics that need to be included in the preform model were to be able to model each tow explicitly, include the effects of friction between the tows, fiber angle jamming and also, incorporate the modeling of sliding to capture the true deformation behavior of the preform. The approach used to represent all these features into the model was to model them one by one, i.e. get one of the features working in the model and then build onto this model to incorporate the rest of the features successfully. This stepwise procedure followed in the formulation of the model is outlined in the following section. Each model is explained with its features and its limitations.

2.4.1 Rack Edge Pinned Model

The friction in the tows was modeled as a first step towards the complete model building. The unit cell for this model is shown in Figure 10. The unit cell is formed of 1 shell element and 4 truss elements. The shell elements and the truss elements both are modeled as isotropic materials. The shell element modeling the transition medium is shaped like a rhombus with the tows going along the sides and pinned at the corners. The tows in this model are connected at their point of intersection, i.e. they have a common node at the intersection and as a result they cannot slide with respect to each other.

The tows are modeled explicitly as they are in the preform using 3-D truss elements. The shell elements are required in this model due to the fact that there is no stiffness to flexural loading of a pure truss element. The inclusion of the shell elements overcomes this problem and also allows for modeling the effect of friction between the tows. In this way the shells provided the initial stiffness to the tensile extension of the preform.

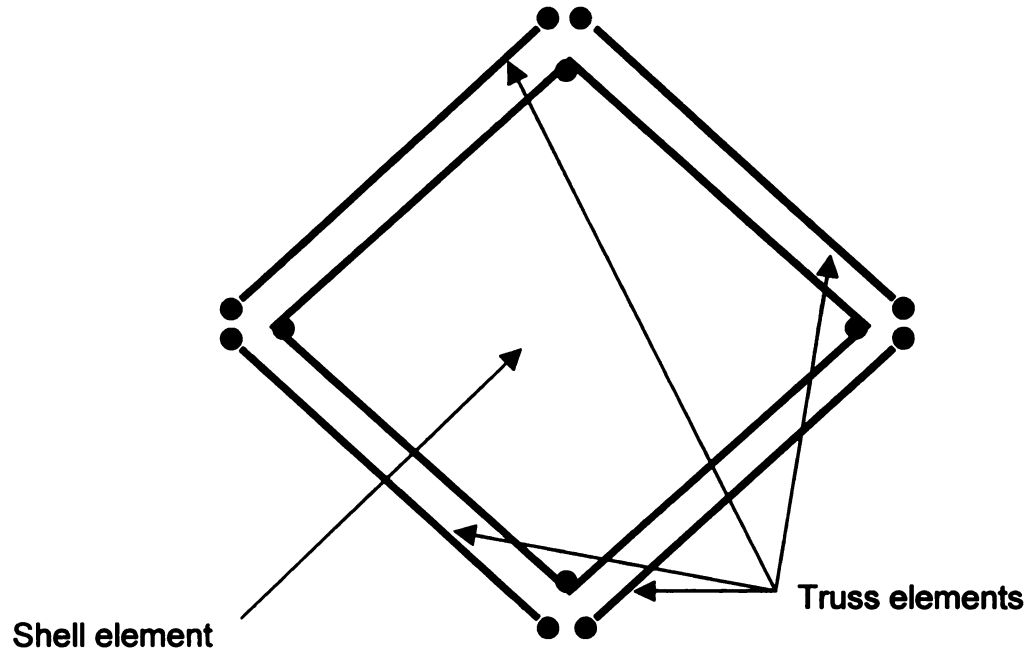

Figure 10. Unit cell for the rack edge pinned model. The figure shows the elements at a reduced scale and separated to show the connectivity. Dark circles indicate nodes.

The effect of the friction between the tows is modeled through the stiffness of the shell elements. The unit cell and the entire modeled preform are shown below in Figures 10 and 11 respectively. This model is called the Rack Edge

Pinned model as the edges of this model resemble the teeth of a rack in rack and pinion and the tows are pinned.

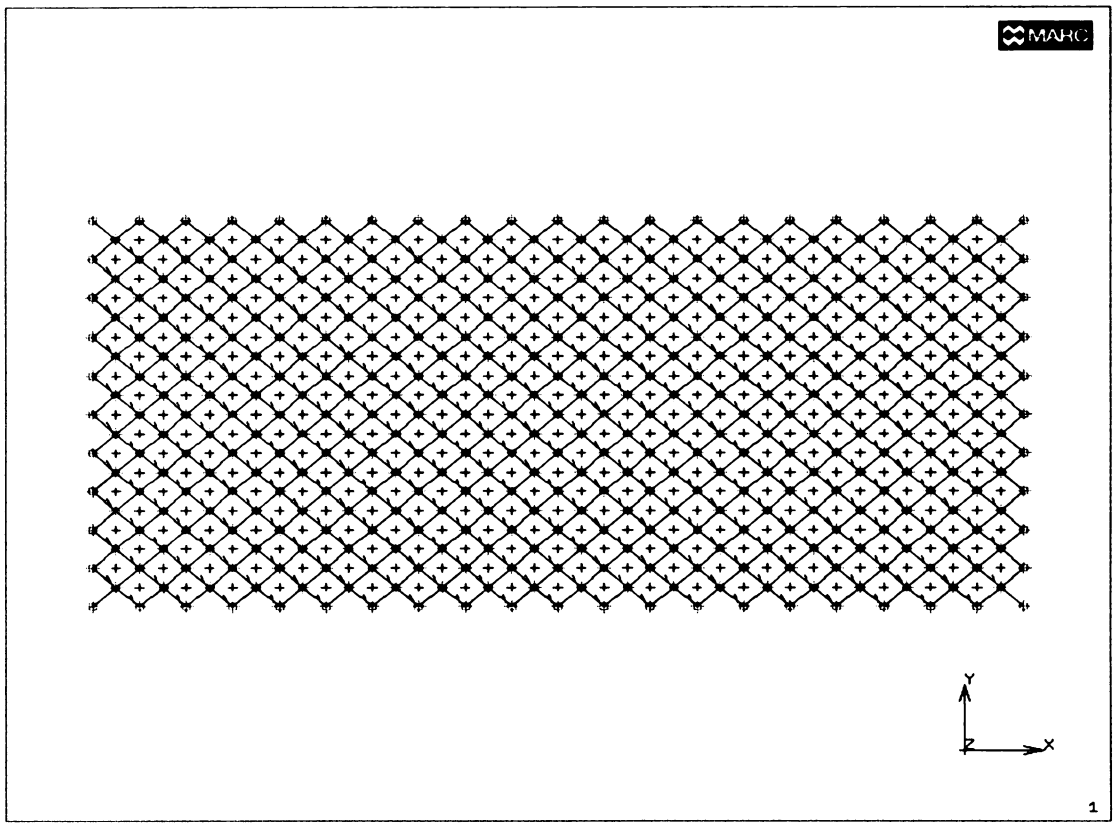

Figure 11. The complete assembled preform for the rack edge pinned model.

The main drawbacks and limitations of this model are: -

1. There is no fiber angle jamming allowed in this model.
2. Also, it does not allow for the inter tow sliding as the tows are pinned together at the intersection.

The next step was to include the fiber angle jamming into the model. Inclusion of the feature of representation of the jamming was accomplished by

using a non-linear material with a stiffening behavior. The Mooney-Rivlin material model was used for the shell elements. The main purpose of using this material model for the shell elements is that this material stiffens up with increasing strain. The shear stress strain curve is shown in Figure 12.

This was the kind of material model that was needed for the shell elements to model the tow jamming in the model. The deformation mode for the shell elements in this model is primarily shear as shown in the Figure 13.

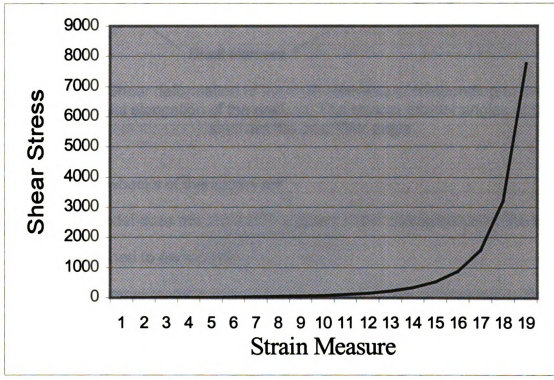

Figure 12. The shear stress-strain curve for the mooney-rivlin material. The shear strain values are not absolute shear strain values but increment numbers for the incremental shear strain application.

The material parameters used in defining the Mooney-Rivlin material model were varied until the deformation behavior and the fiber angle change with

percentage elongation matched the experiments. The results were compared with those from the work of Mauget et al. [12]. The details of the analysis and the results are discussed in the results' section in Chapter III.

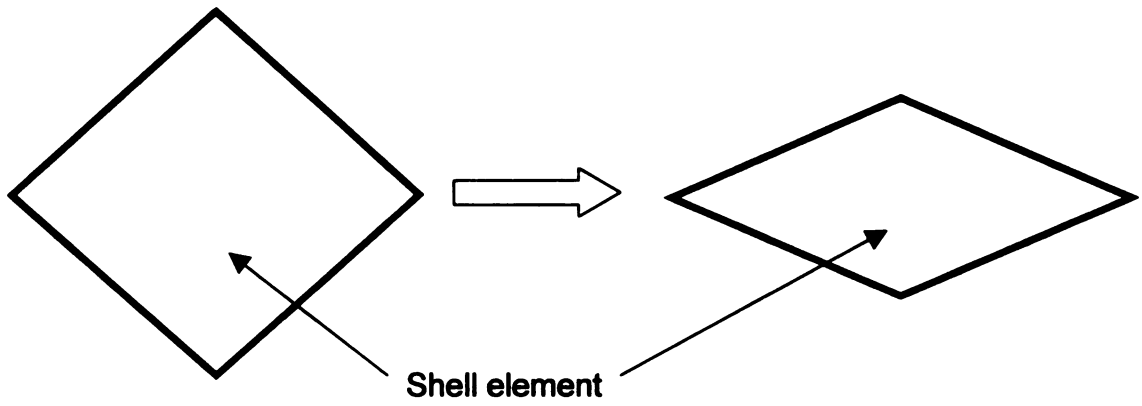

Figure 13. Shear deformation of the shell elements corresponding to the uniaxial elongation of the preform. The smaller interior angles of the shell are the inter fiber angle.

The main drawbacks of this model are: -

1. this model does not allow the modeling of the sliding behavior the tows are pinned to each other.
2. the material model needs to be simple and easily understood so that it is easier to recover the experimental data with varying very few material parameters.

2.4.2 Rack Edge Sliding Model

The next step was to include the sliding behavior of the tows into the model while still maintaining the explicit modeling of the tows in the preform. This was accomplished by meshing the preform in a particular way such that no two

tows are connected together directly i.e. they do not have a common node. The overall connectivity of the entire preform is maintained through the shell elements, which indirectly connect all the tows to each other. In the complete model, individually, each tow runs independently of all the other tows i.e. at no point on the tow is it directly connected to any other tow. No two tows have any common node between them. This property of this new mesh provides it with the ability to model sliding behavior of the tows during deformation of the preform. These changes were incorporated into the initial rack edge model. This model is called the Sliding Rack Edge model. The unit cell of this model is shown in Figure 14, and Figure 15 shows the assembled preform mesh. The unit cell consists of 4 truss elements and 4 shell elements. The connectivity of the truss elements to the shell elements is shown in Figure 16.

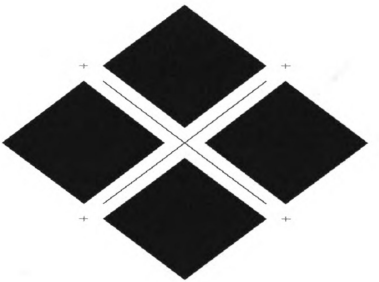

Figure 14. The unit cell of the rack edge sliding model. The plus marks in the figure show the displaced nodes of the truss elements. The figure shows elements at 80% of their actual size.

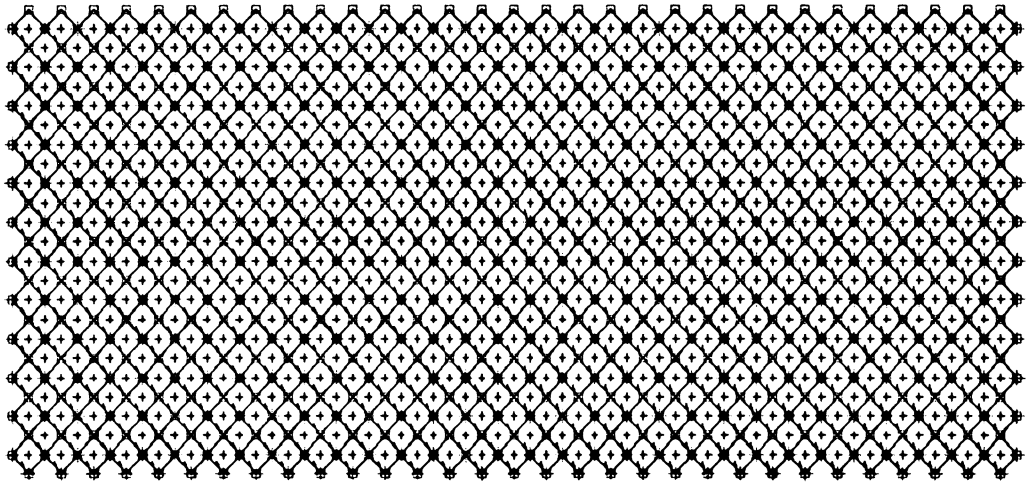

Figure 15. The complete modeled preform for the rack edge sliding model.

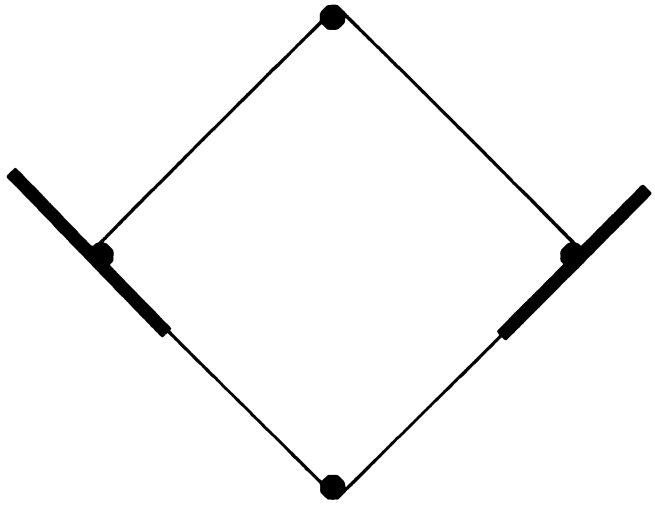

Figure 16. The connectivity between the shell elements and the truss elements. The dark circles are the nodes of the shell element. The dark lines represent the node at which the tows are connected to the shell and the direction.

The main drawbacks of this model are: -

1) at the edges of the modeled preform two adjacent tows have no shell element between them and hence there is no support to these elements which results in extreme deformations at the edges.
2) The jamming behavior can be modeled using the shear modulus of the shell elements but it is difficult to identify the local shell element strains related to the overall sliding behavior in the preform.
3) The shell elements are not connected to any truss elements at one interior node and this results in strange deformation modes in the elements leading to element warpage. Also since the local deformation behavior is not identical in all the elements it is difficult to come up with a unique material constitutive law for all the transition medium elements.

After trying all the above-mentioned models and finding the inadequacies of these models the following three basic rules have been identified that need to be followed while developing the preform model.

1) **Uniformity**. The unit cell model for the preform should be defined such that each shell element in the model is identical to the others in terms of the number and type of tow (truss) element connections. The shell elements may differ only by a simple rotation about the shell normal. This is necessary to ensure that one material law can be defined for all the shell elements.
2) **Support at every node**. The shell elements should be connected to a tow at all its nodes. This is necessary in order for the shell elements to

have a realistic deformation mode and to avoid extreme deformations that may result when there are unsupported nodes in the shell elements.

3) **Connectivity**. The connectivity of the elements should be such that no two tows have a common node. In other words, all the tows are independent of one another, and they interact only through the shell elements.

2.4.3 Tongue and Groove Model

Using the above-mentioned rules the Tongue and Groove model was developed, which is free of all the shortcomings and errors of the models discussed earlier. The complete configuration of the unit cell is shown in Figure 17, and Figure 19 shows the model of the whole ±45° plain weave preform using the tongue and groove model. In Figure 17 the nodes for the shell elements have not been shown for clarity. As can be seen, the unit cell is made up of 4 two noded line elements and 4 four noded quad elements. The unit cell in the figure shows the elements at 90% of their actual size to give a clear view of the way the elements are connected. The line elements represent the tows of the preform and the quad elements have been used to model the fictitious material between the tows, which we already have defined as our transition medium.

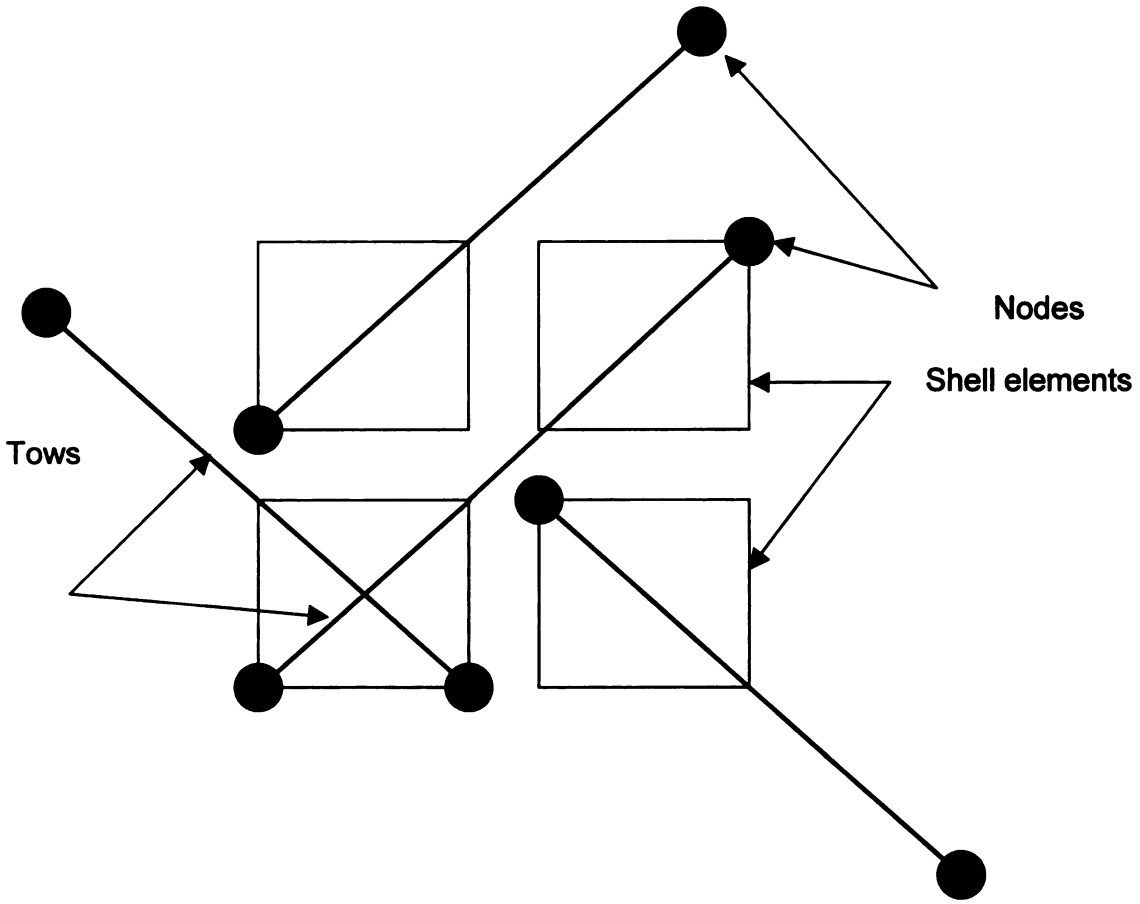

Figure 17. The unit cell for tongue and groove model

The connectivity at the nodes showing the sameness and the support at all nodes is shown in Figure 18. The lines in this figure represent the tows in the direction of the lines and they are connected at the node that they pass through. The uniformity can be seen in the complete model Figure 19 as any shell element in the model differs from this element by just a rotation. Also each shell element has a tow connected to each of its nodes.

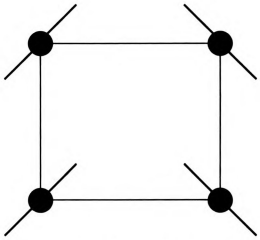

Figure 18. The tow-to-shell element connectivity in tongue and groove model

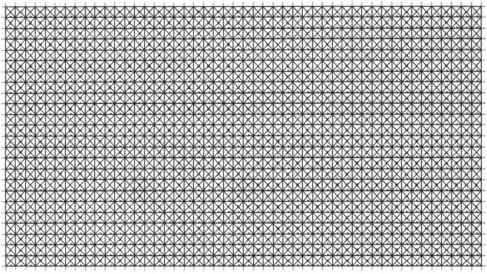

Figure 19. The complete modeled preform for the tongue and groove model.

The four line elements in the unit cell are not connected to each other, i.e. they do not have any common node. The connectivity between the various tows is formed through the shell elements, so the various tows interact only through

the transition medium. As a result of this when the whole of the preform is modeled with the unit cells, each line element is part of one continuous tow and each tow is free from all the other tows. This property of the mesh gives us the means to incorporate inter tow sliding into our model, as the tows are not pin jointed. Although this model satisfies all previously mentioned criteria of uniformity, support at all nodes and connectivity, there were some poor mesh deformation issues with using this model due to lack of symmetry about the tows. Due to this lack of symmetry, the shell elements deform in a cyclic non-uniform mode. This is shown in the results section in the pictures of the stretched preform modeled using the tongue and groove model. Because of this, a new model, called the checkerboard model was developed.

2.4.4 Checkerboard Model

The unit cell for the checkerboard model is shown in Figure 20 and the complete model of the preform is shown in Figure 22.

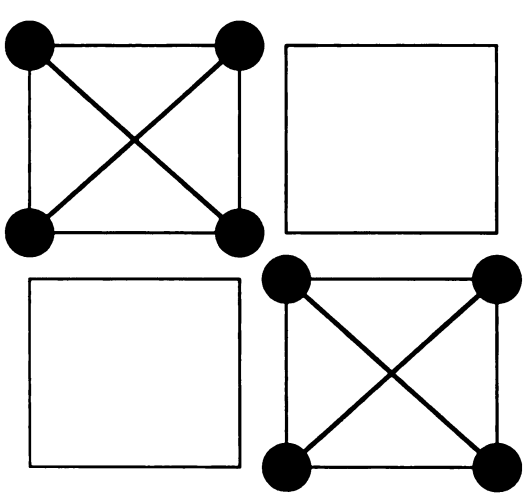

Figure 20. The unit cell for the checkerboard model

In this case the model meets the support at all nodes and the connectivity criterion completely and almost meets the uniformity criterion. Figure 21 shows the two types of shell elements that exist in the complete model. These two cases are not exactly the same but they are similar enough to give a uniform deformation mode for the shells. This model satisfies the uniformity law as this rule was selected so that the elements of the transition medium deform in a similar fashion allowing the use of a simple and easy constitutive material model for all the transition elements. Also the assembled model contains symmetry in both the transverse and the axial directions. As a result of the symmetry in the model, the non-uniform deformation modes that appeared in the deformed model of the preform with the Tongue and Groove model do not appear in the stretched preform modeled with the checkerboard model.

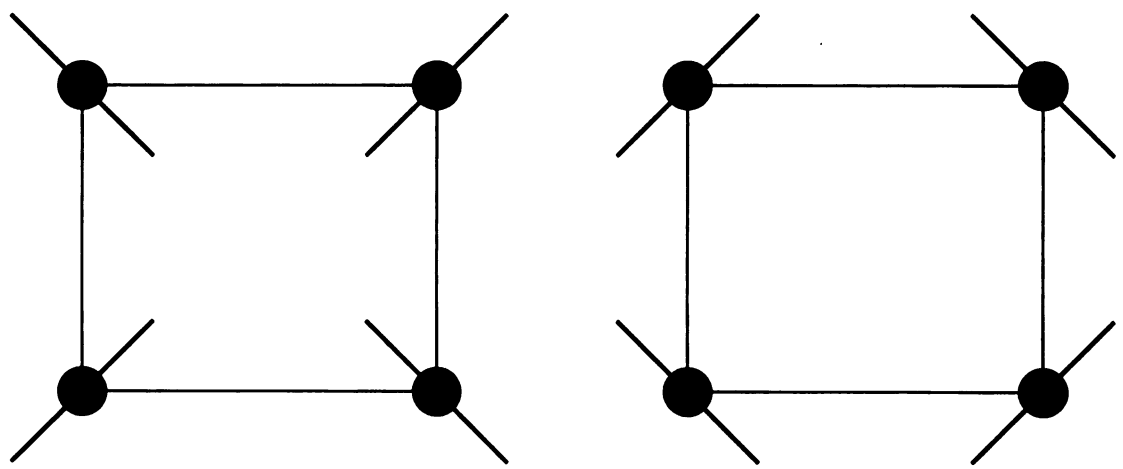

Figure 21. The two types of tow-to-shell element connectivity in the checkerboard model.

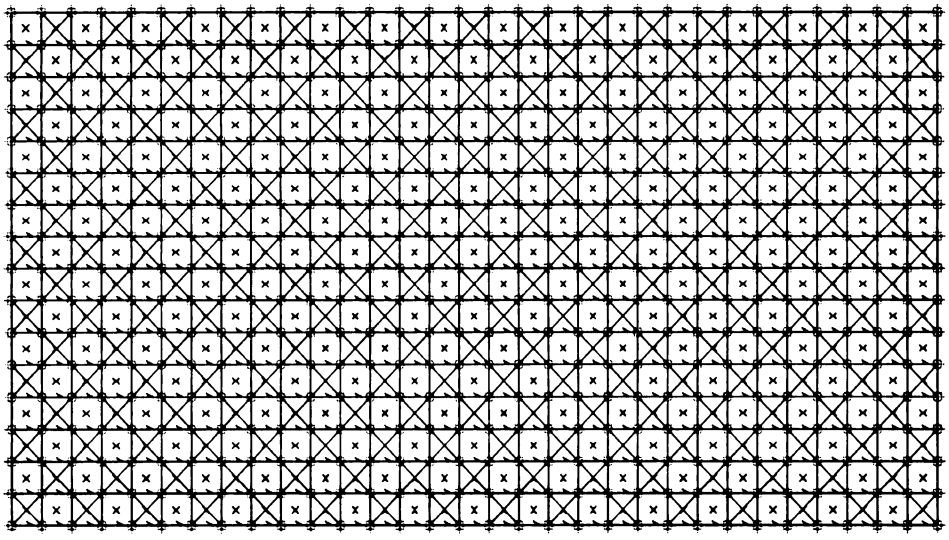

Figure 22. The complete modeled preform for the checkerboard model.

The straightening of the tows from their undulating initial form has been neglected. The tows have therefore been modeled as straight two noded truss elements. The tows, which have been modeled as isotropic, have been assumed to have a Young's modulus equal to the Young's modulus of the individual fibers, which has a very high value as compared to the stiffness of the Transition Medium even after the jamming angle has been reached. Hence, the tows are practically inextensible. As a result, even though the strains in the overall preform are very large, the strains in the tows themselves are insignificant during the actual stamping or draping processes.

The Transition Medium in the preform mesh is a critical part of the current model. It is through this fictitious material that the effects of all the tow

interactions, during the deformation, of a preform have been modeled. The fabric deformation can be divided into 3 stages: -

1) the pre-jamming stage;

2) the jamming stage; and

3) the post-jamming stage.

In the pre-jamming stage, deformation is primarily due to the scissoring action. During this stage the only resistance to the deformation comes from the friction between the tows as they rotate on the surface of other tows. The magnitude of this frictional resistance is relatively small magnitude and deformation within the stage can be produced without the application of high loads. As the fiber angle gets smaller, it approaches the initial jamming angle at which point the fabric becomes stiffer, requiring more force to deform the fabric. This is the jamming stage where the stiffness of the fabric increases with the deformation and the fiber angle change is small compared to that in the previous stage. This occurs until the final fiber jamming angle is reached. This marks the beginning of the post-jamming stage. In this stage the deformation is primarily due to inter fiber sliding and some scissoring in the regions where the fiber angle is still less than the final fiber jamming angle. This stage is appreciable only during processes involving large deformations, which involve large fiber angle changes.

2.5 Constitutive Model

This section discusses the constitutive material models used for the truss and the shell elements in the checkerboard model. The current model takes into

account the effects of friction, sliding and fiber angle jamming and these effects are modeled into the checkerboard model through the material model of the shell elements. The tows have been modeled as an isotropic material with the stiffness properties equal to those of the fibers. The material law for the transition medium has been formulated from the analysis of the above-mentioned stages to represent the tow interactions of the preform in a simple and accurate way. The stiffness of the shell elements is much less than that of the truss elements, i.e. the tows, and as a result the tows are practically rigid relative to the transition medium. This is due to the fact that the shell elements represent only the effects of friction, jamming and sliding which are very small as compared to the axial stiffness of the tows. Normal strain in the shell elements represent the tow scissoring as has been shown in Figure 3 whereas sliding deformation requires the shell elements to undergo shear deformation, which has been depicted in Figure 5.

The material law for the transition medium is assumed to be non-linear orthotropic. The criterion used for determining the normal stress strain curve is that the stiffness of the transition medium is increased first when the fiber angle reaches the initial jamming angle and then, finally increased again when the fiber angle reaches the final jamming angle. The normal stress-strain relationship for the shell elements is shown in Figure 23.

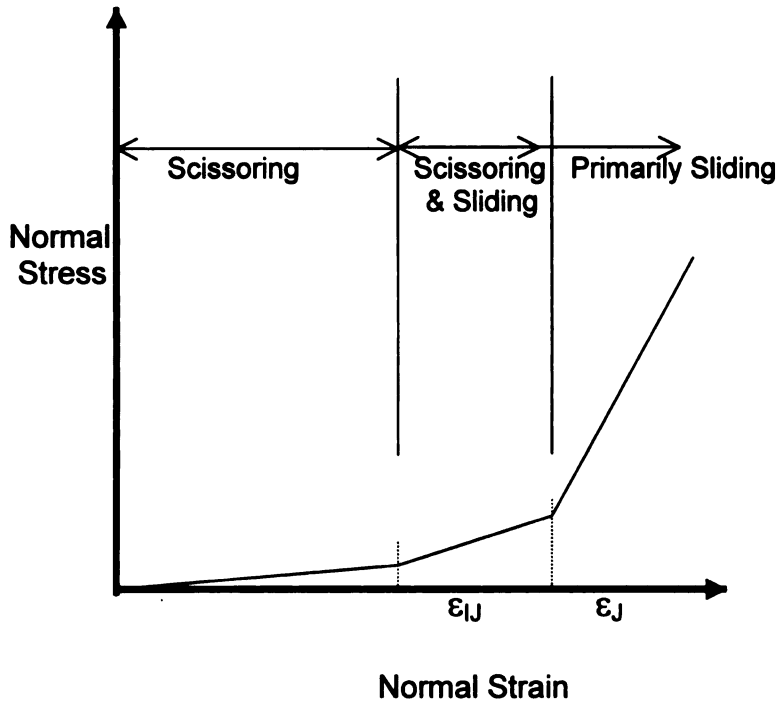

Figure 23. The normal stress-strain curve for transition medium

The relationship between E, G and ν for isotropic materials is not necessarily satisfied. The compressive behavior of the tows is not considered at this time. The curve for the normal stress-strain relationship is tri-linear. The first part of the normal stress-strain curve represents the inter tow friction, which is the resistance to scissoring. The second part marks the beginning of the phase in which the adjacent parallel tows are in contact with each other, i.e. the deformation between the initial fiber jamming angle and the final jamming angle. The first transition point on the curve corresponds to the axial strain in the shell element when the angle between the tows passing through this shell element is equal to the initial fiber jamming angle. After reaching this point the stiffness of the shell element increases. This also marks the increase in the force required to

deform the fabric through scissoring, which now requires the change in the tow width together with the friction between the tows.

The third part of the normal stress-strain curve marks the end of scissoring in this local region, as the stiffness associated with further change in the width of the tows is very high. As a result, any further deformation of the fabric is not due to scissoring but rather due to the inter tow sliding. This is due to the fact that it now takes more energy for the fabric to deform through scissoring of the tows, which now requires a further change in the tow width, which is already reduced from the initial width, than to deform through inter tow sliding. The Elastic moduli for the first, second, and the third part used for the shell elements are 10,20 and 190 psi respectively. The shear modulus of the transition medium is an indirect measure of the resistance to inter tow sliding because in order to facilitate sliding between the tows, the shell elements have to deform primarily in the shear mode. The value of the shear stiffness is chosen such that the value is more than the initial normal stiffness but less than the final normal stiffness of the shell elements. The shear modulus used for the shell elements is 60 psi. The shear modulus of the transition medium is assumed to remain constant throughout the deformation. The shear stress-strain relationship is shown in Figure 24.

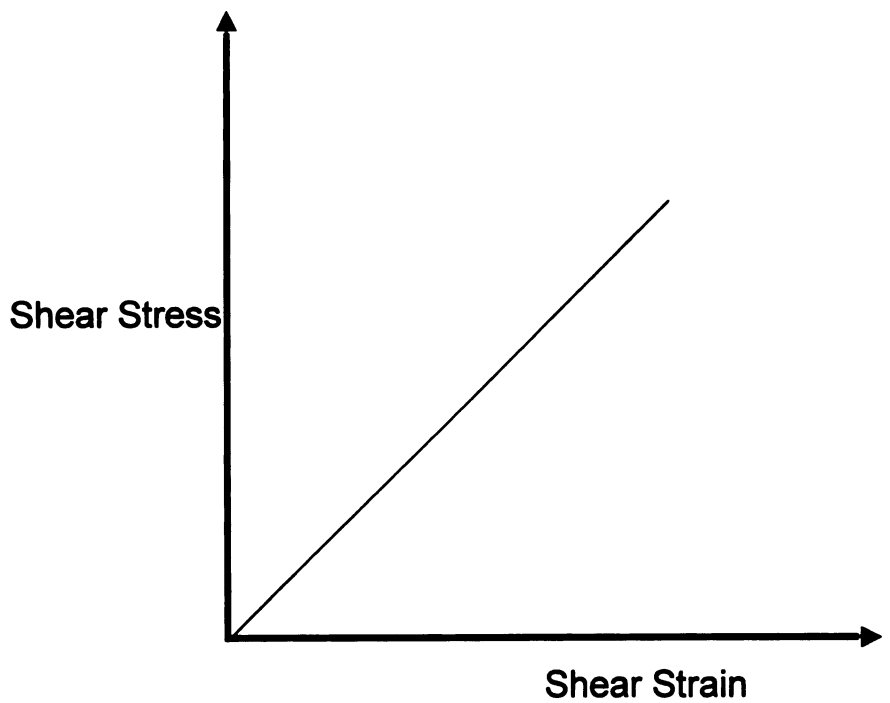

Figure 24. The shear stress-strain curve for the transition medium

The uni-axial tensile test on the specimen provided the overall behavior of the whole preform as well as the means to calibrate the constitutive law for the transition medium. This was done by calculating the approximate of the initial stiffness of the shell elements from the initial linear part of the force deflection curve from the experiment, as during this part the deformation is primarily due to scissoring. This was done by calculating the stress during the initial part using the thickness of the tow and the width of the preform as the dimensions of the cross-section. Further it was assumed that the middle portion of the perform,

which deforms primarily through scissoring (third zone, the zones are described later) takes almost all (about 90%) of the overall strain of the fabric, within this linear initial part. So the strain in this region is calculated from the total strain in the preform. These stress and strain values are then used to calculate the approximate initial stiffness of the transition medium. The stiffness values for the second and the third part of the normal stress-strain curve are assumed since the deformation now involves more complex local behavior due to the formation of different zones, which is explained later. Performing the uni-axial extension simulations using the approximate and the assumed values for the stiffness of transition medium establish the final stress-strain law for the transition medium. The force deflection curve for the whole preform is plotted for the results from each simulation. Thus the final stress-strain curve for the transition medium was established by trial and error until the original force-deflection curve from the experiment is recovered.

Chapter 3

3 EXPERIMENTATION AND NUMERICAL RESULTS

Various sets of experiments were performed to first get an understanding of all the different local deformation behaviors in the tows to be able to accurately model the overall behavior, to validate the model and then to show its use in stamping and draping processes.

3.1 Large Scale Local Model

A large-scale model of a part of the plain weave preform was built to study the behavior of the tows at a finer level for a better understanding of the deformation. 0.2-cm diameter plastic trimmer line was used to build tows that were then braided to form a ±45° plain weave preform. Each tow was built by grouping together about 100 fibers (where fiber refers to a strand of the trimmer line) to get an effect similar to a real tow in a preform. The weave was then fixed in a shear deformable frame made out of C-section steel bars. Special holders were made out of plexi-glass to fix the tows in the frame and also to keep the fibers together. The set up of the apparatus is shown in Figure 25. The apparatus was then sheared to effect a change in the fiber angle, which was initially at 90°. It was noticed that the change in fiber angle after the tows come in contact with each other involves change in the width of the tows as has been mentioned earlier. The jamming of the fiber angle was also studied and the increase in the

force required to shear the apparatus after reaching the initial jamming angle was also studied to help understand the force deflection curve from the experiments on the real preform. With good understanding gained into the mechanics involved during the deformation of a perform, experiments were performed on an actual preform.

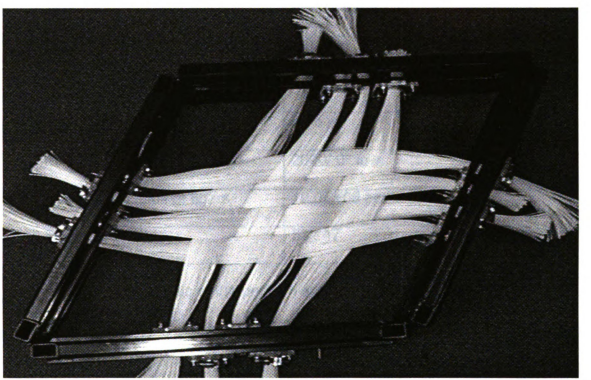

Figure 25. The experimental large scale model of a part of a plain weave preform. The figure shows the tows in a sheared position.

3.2 Uniaxial Experiments

Uni-axial tensile tests were performed on plain weave specimens to formulate the constitutive behavior of the fictitious material from the overall response of the preform specimen. A UTS machine with a load cell of 20 pounds

was used for the tensile tests, as the material S-2 fiberglass ±45° plain weave preform was very compliant. The properties of the material of the preform and the geometric data of the perform specimen used is given in Table1.

Material	S-2 glass
Type	Plain weave ±45°
Tow thickness	0.016 in.
Tow width	0.21 in.
Tow spacing	0.25 in.
Fiber count per tow	2000/ 0° tow
Young's Modulus of fibers	10.0E+06 psi
Ratio 0-90	53 : 47

Table1. Properties of the perform specimen used for experiments.

The preform size used was 8 X 16 in. and the smaller edges were clamped in the jaws of the UTS. The upper jaw of the UTS was then moved at a uniform velocity of 0.2 in/min. A total of 1000 data points were recorded, for the force deflection curve, from 0 to 30% total preform elongation. At this percentage elongation during the tensile experiment the tows start coming out of the preform at the corners of the clamped edges. Moreover the inter tow sliding becomes extreme at this level of elongation. Figures 26 through 29 show the deformed

shapes of the preform at elongations of 10, 15, 20, and 25 percent. The top free edge of the preform starts to form a concave curve and the preform keeps deforming into the shape of a concave lens. This occurs until the fiber angle in the Zone III gets closer to the final jamming angle at which point the preform starts flattening out at the middle part of the free edges since the fiber angle cannot change any further. This starts at around 20% elongation and then the flat part increases in width as the elongation increases. The force versus % elongation curve from the experiment is shown in Figure 30.

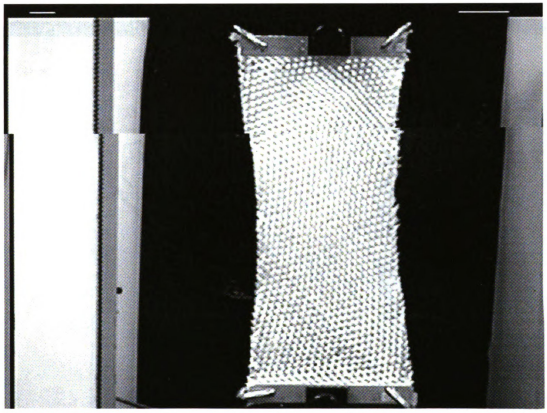

Figure 26. Deformed preform at 10% elongation.

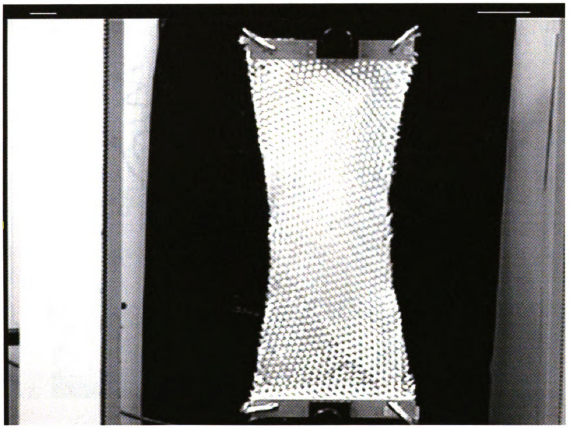

Figure 27. Deformed preform at 15% elongation.

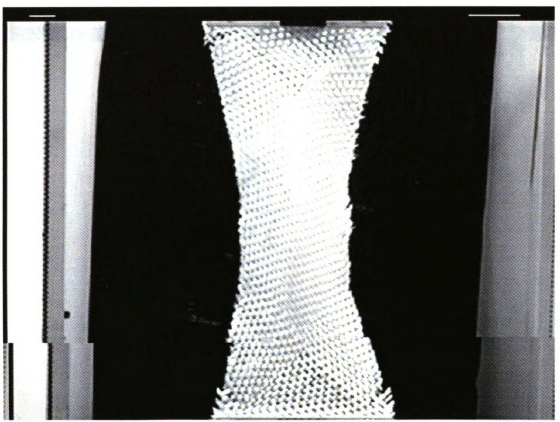

Figure 28. Deformed preform at 20% elongation.

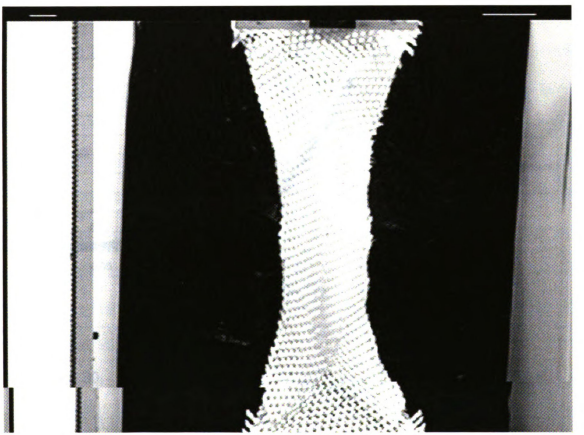

Figure 29. Deformed preform at 25% elongation.

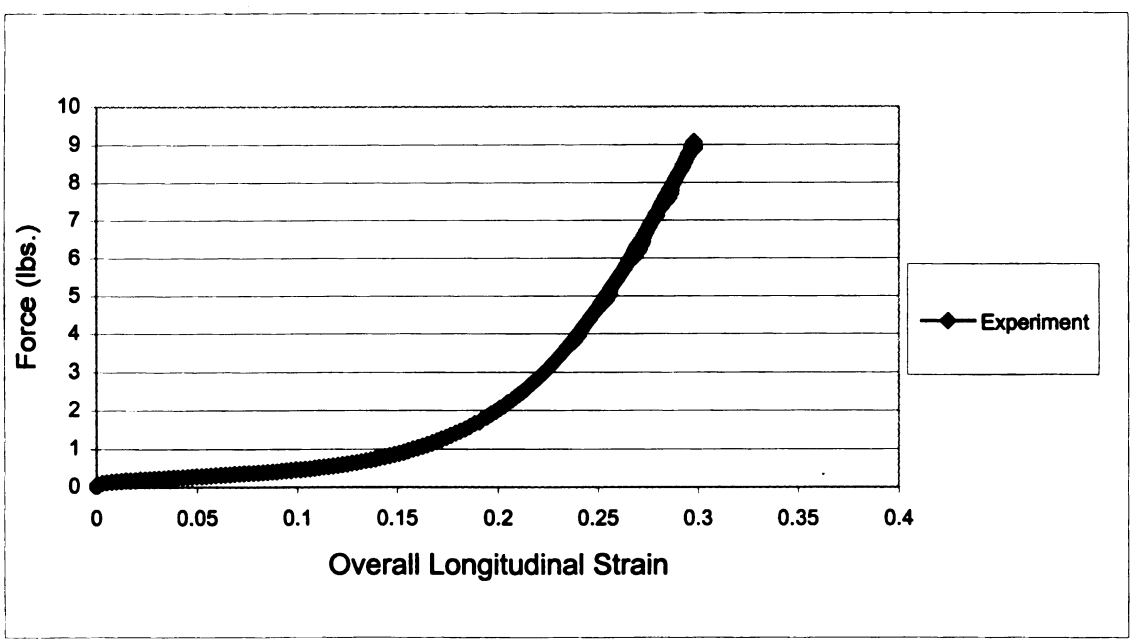

Figure 30. Force versus % elongation of the preform from the uniaxial experiment.

There are distinct zones that form within the preform when it undergoes a uni-axial extension with the ends constrained from displacement in the transverse direction. There are three basic deformation zones that can be identified on the preform and they are shown in the Figure 31 below. The various modes of deformation taking place in these zones are explained below.

Zone I is formed of two isosceles triangles, on each end of the preform, with the base as the width of the preform being held in the clamps and the other two equal sides making an angle equal to one half the original fiber angle between the tows of the undeformed preform. This is the rigid zone. There is no significant deformation taking place in this zone. The fiber angle stays the same as of the undeformed preform and there is also hardly any sliding except on the corners of the base and at the interface with the other zones. This is due to the boundary conditions, as the ends of the preform constrained from moving in the Y and Z directions.

Zone II consists of 4 identical triangular regions, neighboring the zone I. These regions still see some effect of the boundary effects but not as much as the Zone I. In this zone the deformation is a combination of both scissoring and sliding deformation between the tows. There is not a lot of scissoring deformation in this zone, and as a result the fiber angle does not change as much as it does

in the third zone. The sliding deformation is most appreciable at the edges, even though there is some sliding throughout this zone

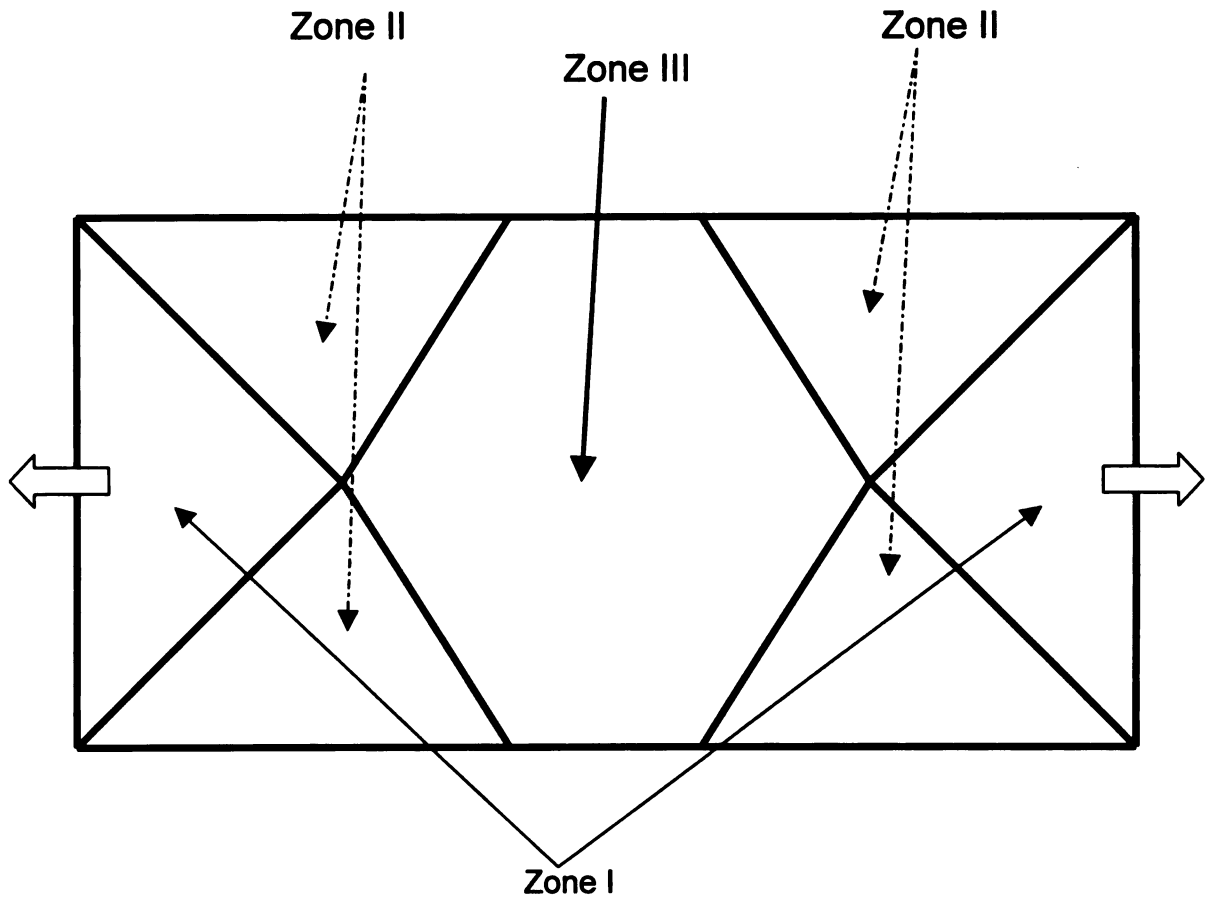

Figure 31. The various Zones formed in a Preform during the Uni-Axial extension

The Zone III is the remainder of the preform located between Zone I and Zone II. It forms a shape that resembles a hexagon. This zone is free from the boundary effects due to the constrained ends but exhibits some edge effects due to the free boundary. Most of the deformation of the fabric occurs in this zone. The main mode of deformation in this zone is scissoring. There is pure scissoring

in the middle of the preform and here the tows behave as if they are pinned to each other. However, there is a considerable amount of sliding that occurs between the tows at the free edge of the preform. These three zones were identified in the uni-axial extension experiment and this zone formation compares well with the results from the numerical simulation of the uni-axial tensile test.

3.3 Uniaxial Sliding Experiment

Another type of experiment that was performed was to show the inter tow sliding in the preform. It is shown that the inter tow sliding deformation is not insignificant in large deformation processes like draping and stamping of preforms. The experimental setup is the same as for the uni-axial tensile experiment but here the preform was coated with a very thin layer of red paint, prior to application of any kind of load on it. The area under the tows remained white as the paint did not get deposited on this region, and the white unpainted part of the tows was revealed during inter-tow sliding. The amount of unpainted part of the tows exposed represents the amount of sliding between them. The experiment shows that the most severe sliding occurs at the interface of the 3 Zones and also on the free edges of the preform and some sliding occurs in the Zone II. Zone III showed almost no sliding at all except for at the free edges of the preform. These results are in good correlation with the results from the simulation as will be discussed below. The force required for the same percentage elongation of the preform increased when using a painted specimen, implying that the resistance to sliding had increased since the paint should not

increase any resistance to tow scissoring. The results of the experiments are shown in the Figures 32 through 36.

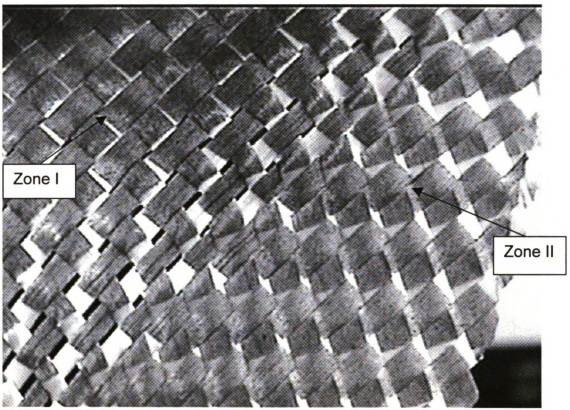

Figure 32. Sliding at the junction of Zone I and Zone II and some sliding in Zone II

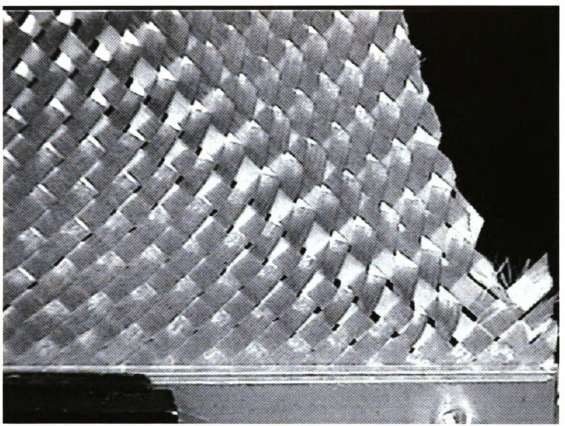

Figure 33. Sliding at the clamped edge at 25% elongation

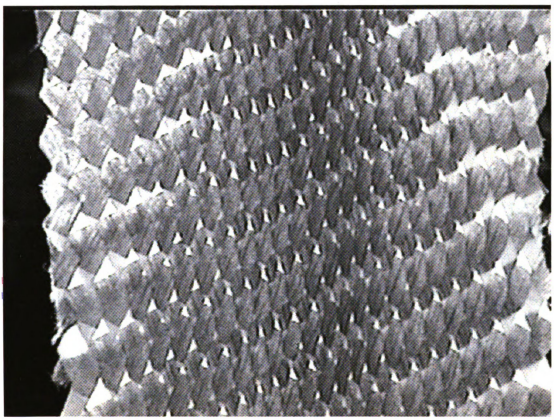

Figure 34. Almost no sliding in Zone III except at the free edges.

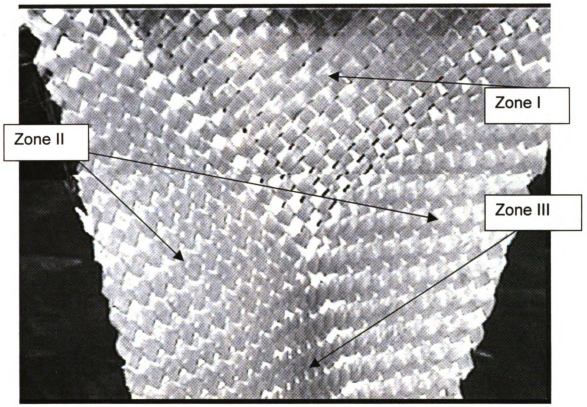

Figure 35. Sliding at the junction of the Zones and some in the Zone II

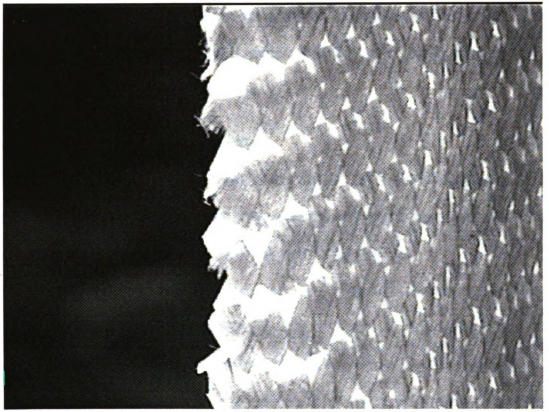

Figure 36. Sliding at the free edge of preform at 20% elongation.

Two different types of analyses, a uni-axial and a draping analysis, were run using the commercial finite element packages MARC and LS-DYNA. The uni-axial simulations were run on MARC and LS-DYNA both to compare the results from explicit and the implicit analysis. The purpose of these simulations was to first check the validity of the FE model and then to simulate the draping analysis of the specimen over a hemisphere using LS-DYNA. The details of the analyses are described in the following sections.

3.4 Uniaxial Tensile Simulation

These simulations were performed for all the models discussed in the model section in Chapter II. The main purpose of these simulations is to check the validity of the model against the experiments performed.

The following conditions are true for all the uni-axial extension simulations. All the nodes were constrained from moving in the out of plane direction. The ends of the modeled preform were constrained in the transverse direction i.e. all the nodes at the two ends had zero displacement in the transverse direction, to simulate the effect of the rigid clamps in the jaws of the tensile testing machine. A fixed, equal and opposite, tensile, incremental displacement was applied to the two ends in the axial direction. These boundary conditions are shown in Figure 37 below. The fiber angles at the center of the preform at different values for the percentage elongation were recorded and compared to the values from the

experiments. The details of these simulations for individual models and the results are discussed in the sections that follow.

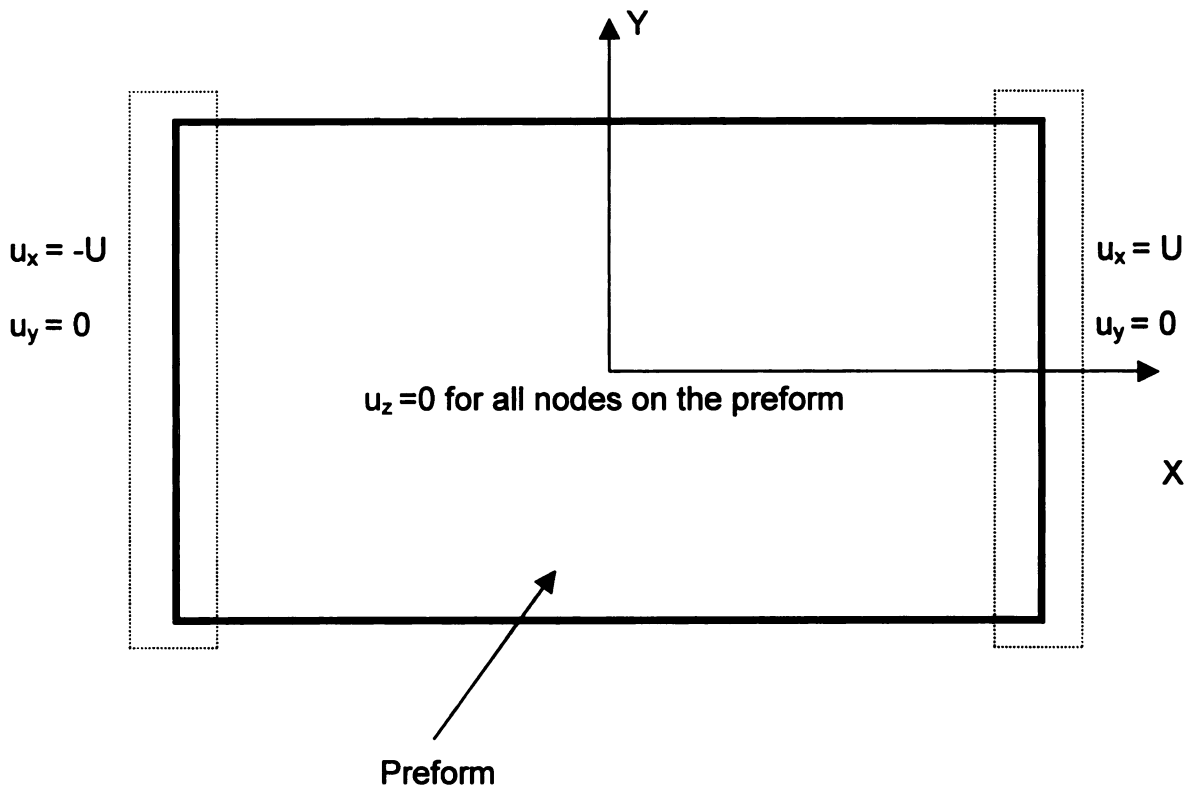

Figure 37. Preform with boundary conditions for the uniaxial test. The dotted rectangle indicates the nodes on the edges of the preform.

3.4.1 Rack Edge Models

The pinned model itself has been discussed in Chapter II under the model formulation. A 8 X 4 in. mesh of a ±50° plain weave composite preform was constructed using this model. Isotropic material model was used for the tows with the stiffness equal to the stiffness of the fibers. These properties of the fibers were taken from [8]. The material model used for the shell elements was Mooney

Rivlin. The material constants were chosen to get the fiber angle to jam at half fiber angle of 18°. The initial part of the curve represents the inter tow friction and the final part represents post jamming behavior. The intermediate part between the two straight lines is the increasing stiffness due to the change in the tow thickness. Figure 38 shows the deformed shape of the preform at 40% elongation.

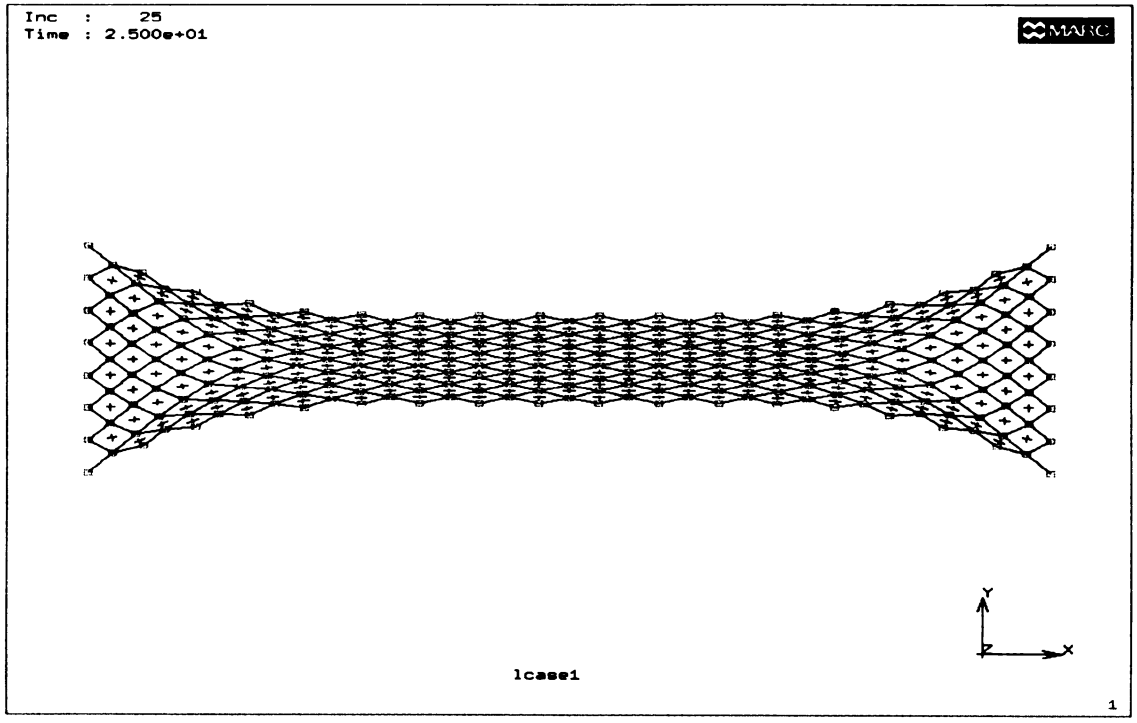

Figure 38. Deformed preform mesh at 40% elongation.

The change in the center fiber angle with % elongation is shown in Figure 39 where it is compared with the data from [8]. The initial part of the curve shows

good correlation with the results in [8] but since their model does not incorporate jamming behavior the fiber angle keeps decreasing to 5° with increasing extension. This is contrary to the experiments, which have shown that the fiber angle jamms between 15-20 degrees half fiber angles.

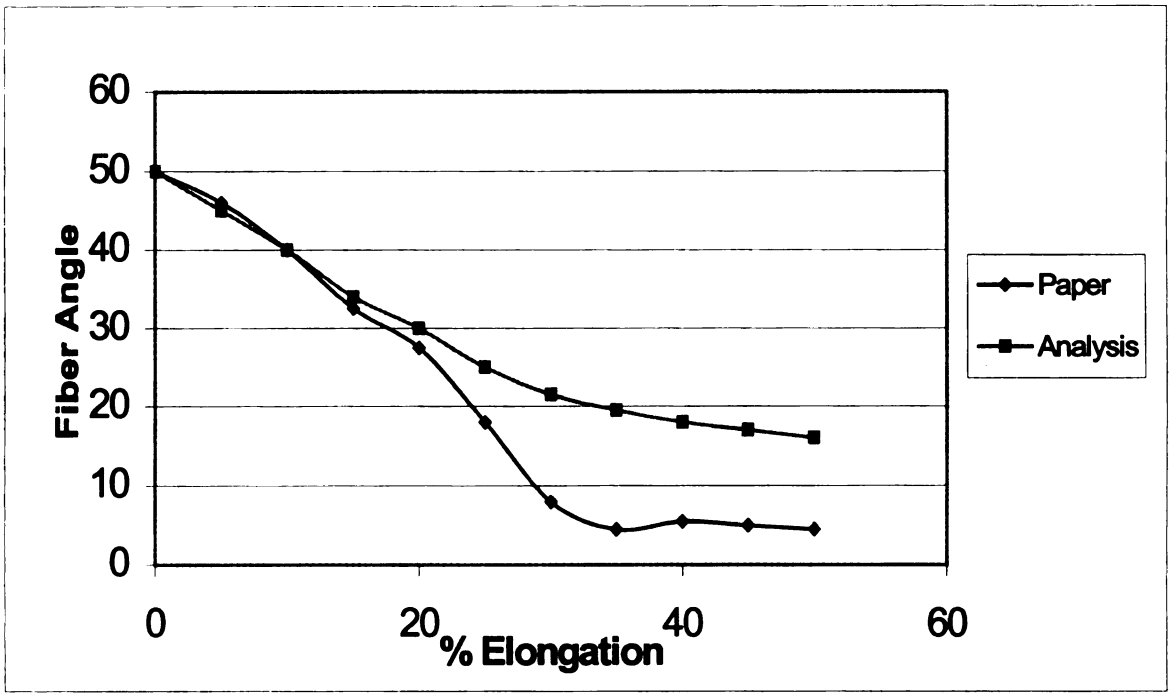

Figure 39. Comparison of center fiber angle from analysis and study by Mauget etal.

The data from the simulation in this study shows the fiber angle jamming which starts at around 30% overall elongation. These results were just qualitative to show that the preform behavior can be modeled accurately using this technique and there was no experimental data to support the results other than the data from [8].

The serrated model with sliding incorporated in it was modeled on the same lines. The results, however, were not accurate due to the drawbacks in this

model, which have already been discussed in Chapter 2. The main reason for not using this model was the asymmetric shell elements, which makes it impossible to represent all the shell elements with a unique constitutive law. Also, the shell elements did not have support at all nodes.

3.4.2 Tongue and Groove Model

An 8 X 16 in. preform, the same as used in the experiments, was modeled using 1223 truss elements and 1153 shell elements. The meshed preform has been shown in Figure 19. The boundary conditions used are the same as in the previous model. As discussed in the previous chapter this model was not used because of the asymmetric connectivity of the shell elements to the tows. This is shown in Figure 40, which shows the deformed preform.

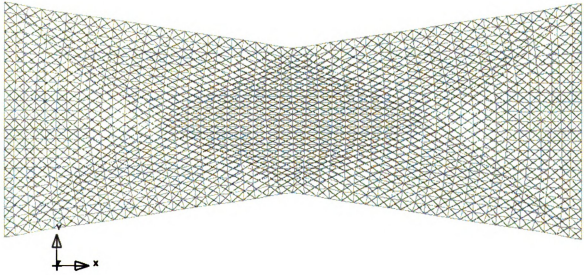

Figure 40. The deformed mesh of preform with tongue and groove model.

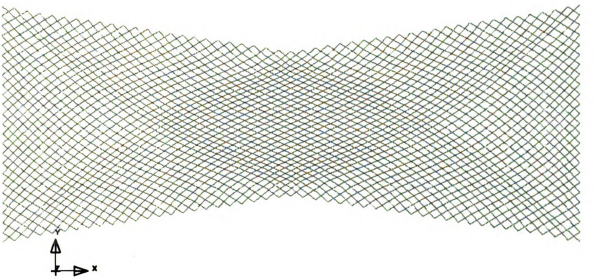

Figure 41. Deformed preform model with only truss elements present.

As can be seen the shell elements see varying normal strain ε_{xx} along the Y direction. The figure 42 shows the varying strain at a larger scale isolated from the complete model. As can be seen in the first column the elements experience increasing compressive strain along the negative Y direction, whereas in the next column of elements it is the other way around. This goes on as we move towards the middle of the preform where the pattern reverses and goes on towards the other end of the preform. This strange deformation mode, which as has already been explained, is due to the connectivity of the shell elements with the tows,

results in an inaccurate prediction of the behavior of the tows during the extension of the preform.

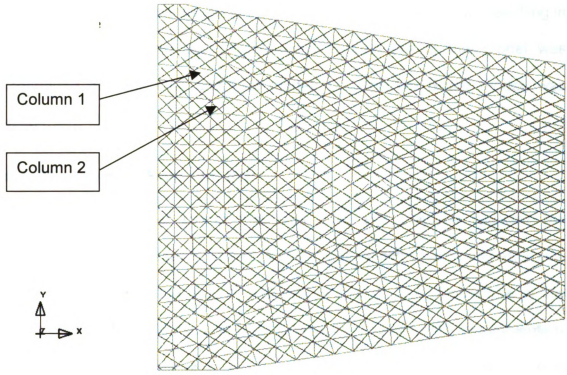

Figure 42. A part of the preform showing the varying strain in the shell elements more clearly (tongue and groove model).

Figure 41 shows the preform with the tows without the shell elements to give a better picture of the tow deformation behavior predicted by this model. No results or comparisons are shown in this model, as the deformation behavior that the model predicted is erroneous. Another drawback in this model is that in order to have a uniform mesh the truss elements at the edges need to be trimmed. This is due to the model characteristics as the length of the truss elements is twice the length of the diagonals of the shell elements. As a result of this the

model of the preform could not represent sliding at the edges since the tows had to be pinned at the point of intersection at the edges. Moreover, the deformation shown in Figure 41 is the maximum deformation that the preform underwent before the analysis died because the element size became very small resulting in an extremely small time step. As a result, further use of this model was discontinued and the new and final model, the Checker Board model, was formed.

3.4.3 The Checker Board Model:

This is the final model that was built and validated against the experimental data. The same type of preform was modeled using this approach as was modeled with the tongue and groove model. The dimensions of the preform are 8 X 16 in. The actual preform specimen used for the experiments is S-2 fiberglass ±45°. The plain weave fabric was modeled using 4608 truss elements and 4608 shell elements. The meshed preform has been shown in Figure 22. The boundary conditions again are the same as described earlier. A maximum overall elongation of 25% was achieved with this model before the simulation died out. This is due to the reason that the sliding between the tows at the free edges becomes large, which is in agreement with the experiments. But as a result of this the shell elements at the edges become warped to accommodate this deformation as they are connected to the tow elements. However, this value of overall elongation is more than sufficient for most of the forming or shaping processes in the industrial applications as reinforcement for a composite part. So this inability of the current model to go beyond 25% overall

elongation is not a limitation of its capabilities as it can be seen that at this elongation there is a significant amount of sliding in the fabric.

Similar patterns of deformation modes were observed in the simulation and experiments. The model predicts the sliding behavior at the same places as shown by the experiments. The predictions are shown in Figure 43 through 46, which are in very good correlation with the results from the experiments showing the inter tow sliding (Figures 32 through 36). Figures 43 through 46 show the mesh of the shell elements with and without the tows since the fiber sliding in the model is predicted at the places where the shell elements undergo considerable shear deformation. The sliding deformation, as predicted by the simulation, is significant along the interface of Zone I with Zone II, the interfaces of Zone II and Zone III and also on the free edges of the preform. The model also predicts some sliding in Zone II, which agrees well with the experiments. Also the interior shell elements in the Zone III undergo only normal deformation indicating pure scissoring behavior.

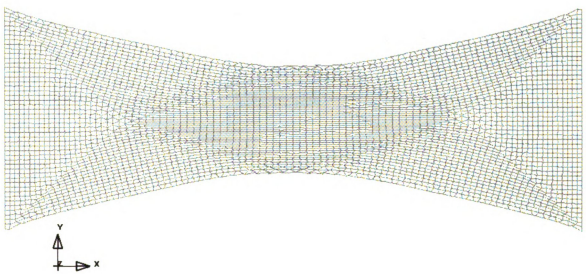

Figure 43. The whole preform mesh with just shells. Shell element distortion indicates sliding.

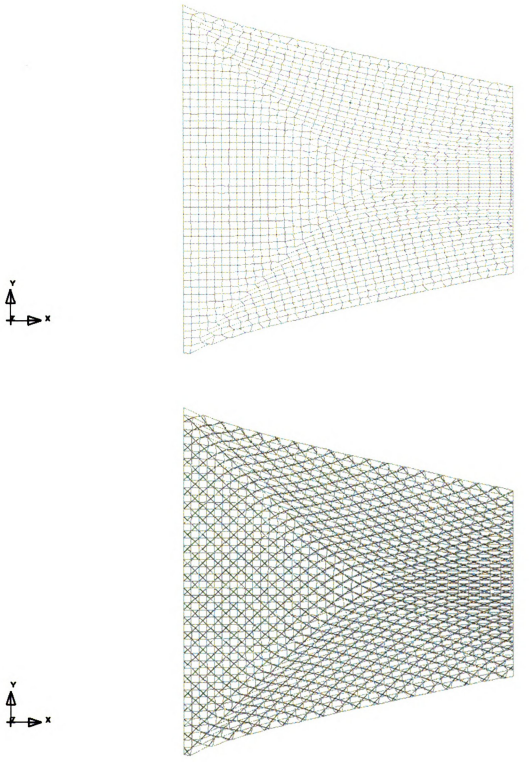

Figure 44. Sliding at the interface between Zones I and II mainly.

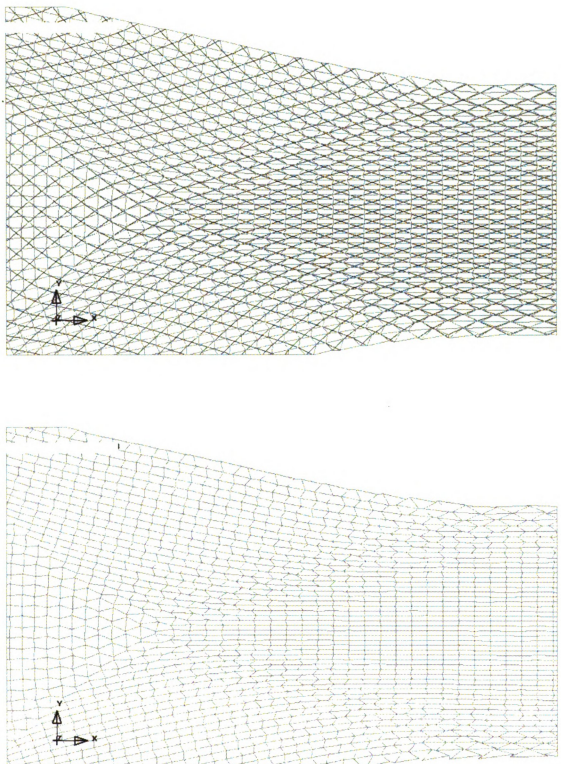

Figure 45. The details of sliding at the interface between Zones II and III.

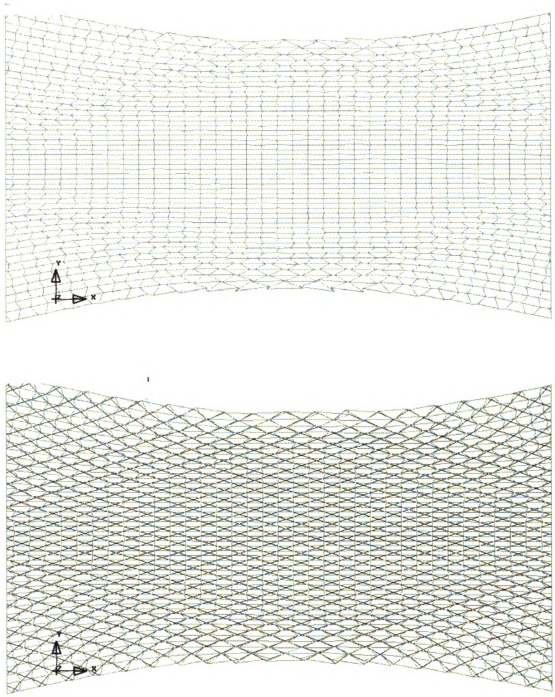

Figure 46. Showing primarily Zone III. All the shell elements deform through normal strain only except the interfaces and the free edges indicating no sliding in the middle and significant sliding at the interface and at the edges.

The overall shape of the fabric at different percentage elongations compared well with the shape of the preform from experiments. Figure 47, 48 and 49 shows the preform at 10, 20, and 25 percent elongation respectively as predicted by the simulation. Figure 50 shows the comparison between the center fiber angles at different percentage elongations from experiments and the predicted angles from the simulation. The figures show that there is good correlation between the experiments and the simulation.

The force deflection curve for the simulation has also been compared with the same curve from the experiments. This is shown in Figure 51, which shows the force deflection curves for both the experiment and the analysis on the same graph. As can be seen the curves are in very good agreement with each other, thus validating the model.

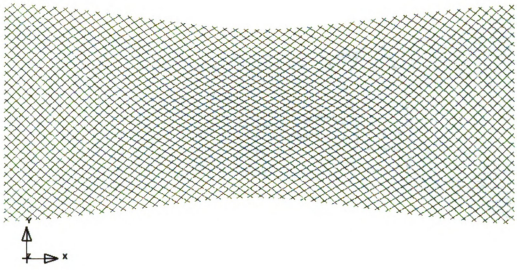

Figure 47. Preform at 10% elongation as predicted by the simulation.

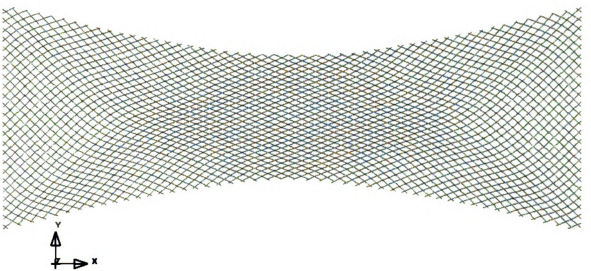

Figure 48. Preform at 20% elongation as predicted by the simulation.

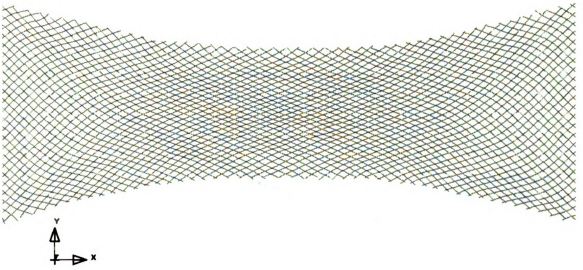

Figure 49. Preform at 25% elongation as predicted by the simulation.

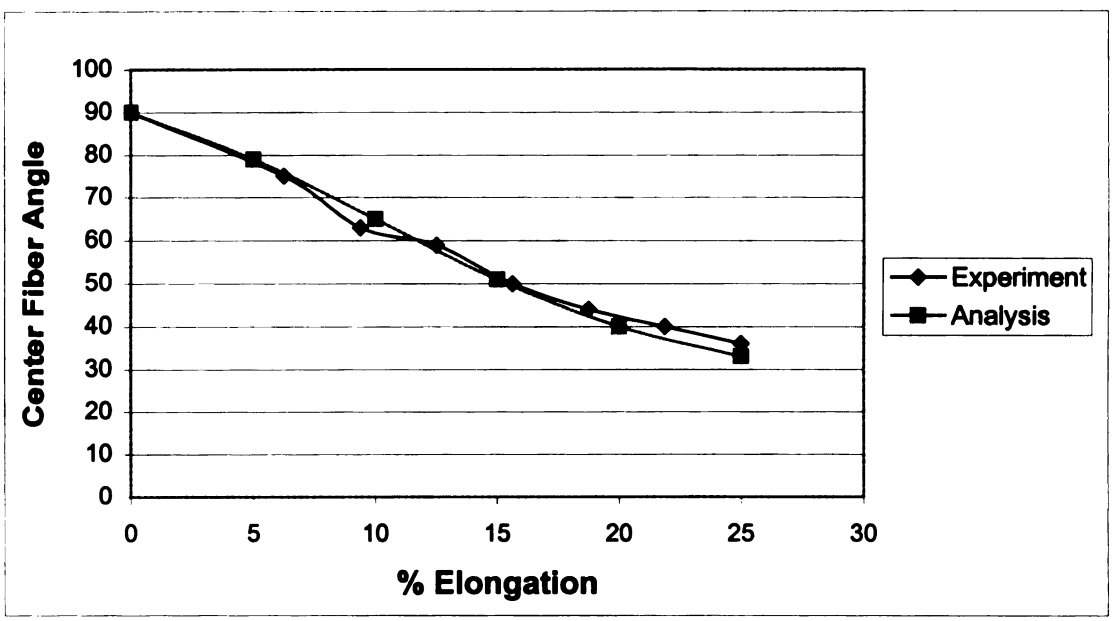

Figure 50. Center fiber angle comparison between experiment and simulation.

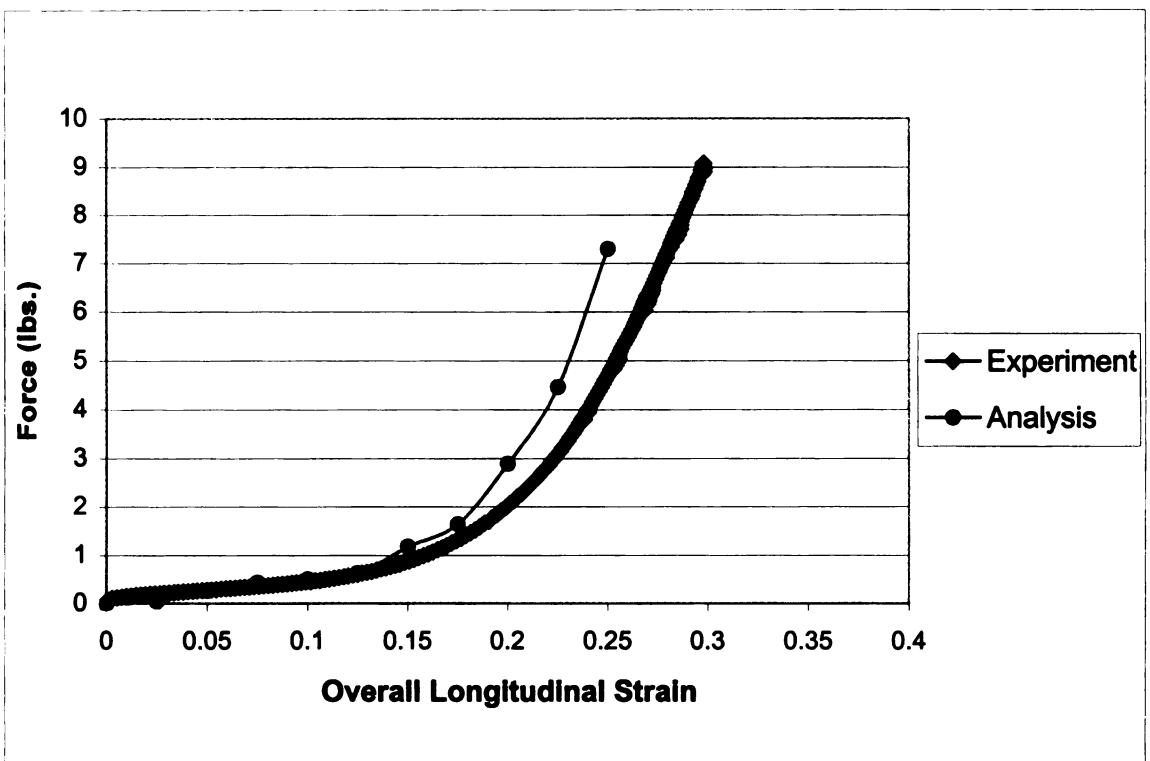

Figure 51. Force versus % elongation plot for experiment and simulation.

3.5 Draping Experiments

The next set of tests was performed using a hydraulic press machine for forming the preform onto a sphere. A spherical punch, with a radius of 2 inches, was used to form the preform. The setup of the machine is such that the working table has a circular hole about 6 inches in diameter. The punch comes from under the table and goes up through the hole. A square plate 10 in. X 10 in. in dimensions, with a cavity of 6 in. X 6 in. cut out of it in the center, was cut out of a hard board to be placed over the preform for support at the edges. The dimensions of the preform sample being formed onto the sphere were 8 in. X 8 in. The preform was placed on the working bench of the machine over the circular hole and the square plate was placed on the preform. Very light weights were placed on the ends of the plate, where there is no preform under it to keep it from lifting under the force from the punch motion into the preform. The boundary conditions were such that the edges of the preform were free to move in all directions except in the direction of movement of punch i.e. vertical direction. The punch was then moved into the preform at incremental displacements of 0.25 in. and pictures of the deformed fabric were taken at different angles. Qualitative results obtained from these pictures were taken and compared with the results obtained from the simulation performed. Figures 52,53 and 54 show the preform contour at punch penetration corresponding to 1.0 in., 1.5in., and 2.25 in. respectively.

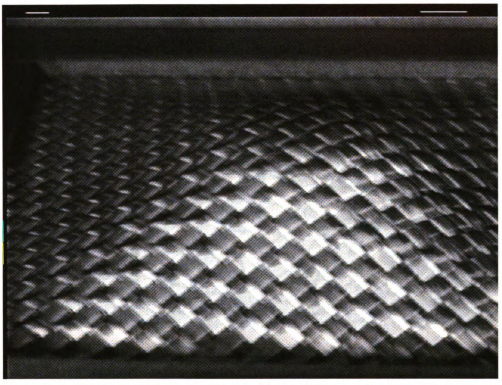

Figure 52. Preform contour at 1 in. penetration.

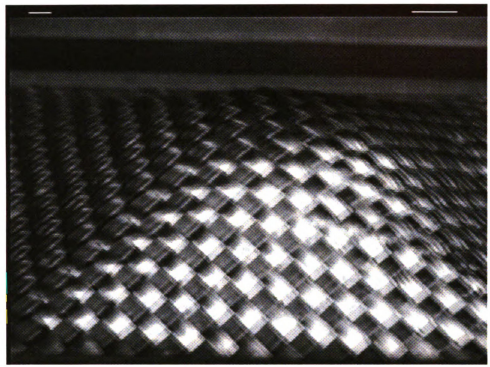

Figure 53. Preform contour at 1.5 in. penetration.

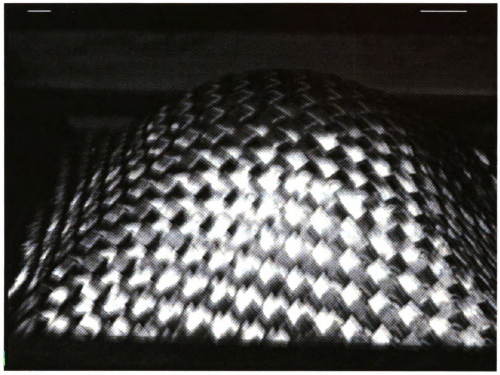

Figure 54. Preform contour at 2.25 in. penetration.

3.6 Draping Simulation

The draping problem was simulated using LSDYNA-3D using the checkerboard model for meshing the preform. The specimen dimensions were 8 in. X 8 in. and it was modeled using 2304 truss elements and 2304 shell elements. The setup for the analysis is the same as for the experiment. The preform is held between two square plates with a 6 in. X 6 in. square hole cut out of the plated to allow the spherical punch to move up into the preform. The preform is free to slide between the plates as the punch moves into it. The radius of the punch is 2 in. The punch is moved into the preform at a uniform speed of 0.3 in./min. The experiment was performed for a total punch penetration of 2.5 in. into the preform. Figures 55,56 and 57 show the preform shapes with the punch penetrations corresponding to 0.25, 1.0, and 2.25 in. as predicted by the simulation. The contour of the preform as predicted by the draping simulation bears close resemblance to the contour shape from the experiments for the corresponding punch penetrations. The figures from the experiments do not show the part of the preform under the square plate placed over the preform. As a result just 6in. X 6in. of the preform, which comes out of the square hole in the square plate is shown. However, for the pictures from the simulation the entire preform is shown i.e. the part under the square plate is also shown. The overall shape of the preform is in good agreement with the experiments.

The fabric deformation is symmetric about the centerline, i.e. the axis of the sphere along its direction of motion. The preform forms a pyramid shape after the punch motion into it with the top rounded, fitting on the punch, and the edges

are rounded. The edges correspond to the preform coming out at the corners of the square hollow in the plate. The simulation also predicts this shape. There is no wrinkling in the preform during the shaping over the spherical punch in both the experiments and the simulation. Almost uniform fiber scissoring occurs along the slanted faces of the so formed pyramid shape of the preform. The fiber angle at the top of the punch does not change and the tows remain essentially perpendicular to each other, both in the experiment and the simulation. The results look very similar in both the experiments and the simulation. This study performed only a qualitative comparison between the analysis and the experiments for the shaping simulation as a good criterion for the quantitative comparison could not be established. It is very difficult to measure the fiber angles on the deformed preform shape in draping process as the faces are slanted. So the comparison of the fiber angles could not be made. However, as said earlier the qualitative results show a good correlation with the experimental results.

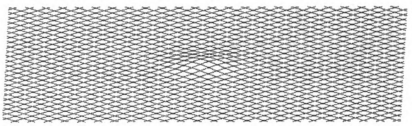

Figure 55. Preform contour at 0.25 in. penetration from simulation.

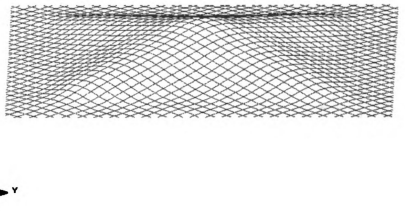

Figure 56. Preform contour at 1.0 in. penetration from simulation.

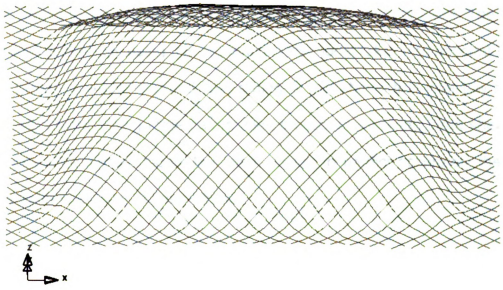

Figure 57. Preform contour at 2.25 in. penetration from simulation.

Chapter 4

4 CONCLUSIONS

A finite element model has been presented for modeling deformation of a plain weave textile composite preform during the stamping process. The preform is modeled explicitly using this approach. This model takes into account the inter fiber friction, tow jamming and fiber sliding. It was shown that inter tow sliding is not insignificant during large deformation processes involving large shear angle changes. The current model has been shown to predict accurately the overall deformation behavior of the preform.

APPENDICES

Appendix A

5 USER MATERIAL CODE

```
      subroutine umat41 (cm,eps,sig,hisv,dt1,capa,etype,time)

      implicit real*8 (a-h,o-z)
c
c     isotropic elastic material (sample user subroutine)
c
c variables
c
c     cm(1)= initial young's modulus
c     cm(2)=poisson's ratio
c
c     eps(1)=local x  strain
c     eps(2)=local y  strain
c     eps(3)=local z  strain
c     eps(4)=local xy strain
c     eps(5)=local yz strain
c     eps(6)=local zx strain
c
c     sig(1)=local x  stress
c     sig(2)=local y  stress
c     sig(3)=local z  stress
c     sig(4)=local xy stress
c     sig(5)=local yz stress
c     sig(6)=local zx stress
c
c     hisv(1)=1st history variable
c     hisv(2)=2nd history variable
c        .
c        .
c        .
c        .
c     hisv(n)=nth history variable
c
c      dt1=current time step size
c      capa=reduction factor for transverse shear
c      etype:
c        eq."brick" for solid elements
c        eq."shell" for all shell elements
```

```
c       eq."beam"  for all beam elements
c
c     time=current problem time.
c
c
c     all transformations into the element local system are
c     performed prior to entering this subroutine.  transformations
c     back to the global system are performed after exiting this
c     routine.
c
c     all history variables are initialized to zero in the input
c     phase.   initialization of history variables to nonzero values
c     may be done during the first call to this subroutine for each
c     element.
c
c     energy calculations for the dyna3d energy balance are done
c     outside this subroutine.
c
      character*(*) etype
      dimension  cm(*),eps(*),sig(*),hisv(*)
c
c     compute shear modulus, g
c
      g2 =cm(1)/(1.+cm(2))
      g  = 60.0
c
      if (etype.eq.'brick') then
      davg=(-eps(1)-eps(2)-eps(3))/3.
      p=-davg*cm(1)/((1.-2.*cm(2)))
      sig(1)=sig(1)+p+g2*(eps(1)+davg)
      sig(2)=sig(2)+p+g2*(eps(2)+davg)
      sig(3)=sig(3)+p+g2*(eps(3)+davg)
      sig(4)=sig(4)+g*eps(4)
      sig(5)=sig(5)+g*eps(5)
      sig(6)=sig(6)+g*eps(6)
c
      elseif (etype.eq.'shell') then
c
         hisv(1) = hisv(1) + eps(1)
         hisv(2) = hisv(2) + eps(2)
         if (hisv(2).gt.-0.45) then
      gc    =capa*g
      q1    =cm(1)*cm(2)/((1.0+cm(2))*(1.0-2.0*cm(2)))
      q3    =1./(q1+g2)
      eps(3)=-q1*(eps(1)+eps(2))*q3
      davg  =(-eps(1)-eps(2)-eps(3))/3.
```

```
      p    =-davg*cm(1)/((1.-2.*cm(2)))
      sig(1)=sig(1)+p+g2*(eps(1)+davg)
      sig(2)=sig(2)+p+g2*(eps(2)+davg)
      sig(3)=0.0
      sig(4)=sig(4)+gc*eps(4)
      sig(5)=sig(5)+gc*eps(5)
      sig(6)=sig(6)+gc*eps(6)
         else
         if (hisv(2).lt.-0.80) then
                        e = 190.0
                        enu=0.3
                        g2=e/(1.0+enu)
                        gc   =capa*g
                        q1   =e*enu/((1.0+enu)*(1.0-2.0*enu))
                        q3   =1./(q1+g2)
                        eps(3)=-q1*(eps(1)+eps(2))*q3
                        davg  =(-eps(1)-eps(2)-eps(3))/3.
                        p    =-davg*e/((1.-2.*enu))
                        sig(1)=sig(1)+p+g2*(eps(1)+davg)
                        sig(2)=sig(2)+p+g2*(eps(2)+davg)
                        sig(3)=0.0
                        sig(4)=sig(4)+gc*eps(4)
                        sig(5)=sig(5)+gc*eps(5)
                        sig(6)=sig(6)+gc*eps(6)
                else
                        e = 20.0
                        enu=0.1
                        g2=e/(1.0+enu)
                        gc   =capa*g
                        q1   =e*enu/((1.0+enu)*(1.0-2.0*enu))
                        q3   =1./(q1+g2)
                        eps(3)=-q1*(eps(1)+eps(2))*q3
                        davg  =(-eps(1)-eps(2)-eps(3))/3.
                        p    =-davg*e/((1.-2.*enu))
                        sig(1)=sig(1)+p+g2*(eps(1)+davg)
                        sig(2)=sig(2)+p+g2*(eps(2)+davg)
                        sig(3)=0.0
                        sig(4)=sig(4)+gc*eps(4)
                        sig(5)=sig(5)+gc*eps(5)
                        sig(6)=sig(6)+gc*eps(6)
                end if
         end if

c
c
      elseif (etype.eq.'beam' ) then
```

```
      q1    =cm(1)*cm(2)/((1.0+cm(2))*(1.0-2.0*cm(2)))
          g=10000.0
      q3    =q1+2.0*g
      gc    =capa*g
      deti  =1./(q3*q3-q1*q1)
      c22i  = q3*deti
      c23i  =-q1*deti
      fac   =(c22i+c23i)*q1
      eps(2)=-eps(1)*fac-sig(2)*c22i-sig(3)*c23i
      eps(3)=-eps(1)*fac-sig(2)*c23i-sig(3)*c22i
      davg  =(-eps(1)-eps(2)-eps(3))/3.
      p     =-davg*cm(1)/((1.-2.*cm(2)))
      sig(1)=sig(1)+p+g2*(eps(1)+davg)
      sig(2)=0.0
      sig(3)=0.0
      sig(4)=sig(4)+gc*eps(4)
      sig(5)=0.0
      sig(6)=sig(6)+gc*eps(6)
      endif
c
      return
      end
```

BIBLIOGRAPHY

6 BIBLIOGRAPHY

1. R.E. Robertson, E.S. Hsiue, E.N. Sickafus, and G.S.Y. Yeh, 1981. "Fiber Rearrangements During the Molding of Continious Fiber Composites. I . Flat Cloth to a Hemisphere" , *Polymer Composites*, 2(3) : 126-31.

2. R.E. Robertson, T.J Chu, M. Park and R.J. Gerard. "Wrinkle Free Preforms for Fiber Composite Structures"

3. Simon Bickerton, Pavel Simacek, Sarah E. Guglielmi, and Suresh G. Advani. 1997. "Investigation of Draping and its Effects on the Mold Filling Process During Manufacturing of a Compound Curved Composite Part", *Composites Part A : Applied Science and Manufacturing 28A*

4. E.M. Sozer, P. Simacek and S.G. Advani. "Draping and Filling of Long Axisymmetric Molds in RTM Process"

5. C.D. Rudd, V. Middleton, M.J. Owen, A.C. Long, P.McGeehin and L.J. Bulmer. 1994. " Modeling the processing and performance of preforms for liquid molding processes", *Composites Manufacturing Volume 5, Number 3.*

6. Bhavani V. Sankar and Ramesh V, Marrey. 1997. "Analytical Method For Micromechanics of Textile Composites", *Composites Science and Technology 57 (1997) 703-713.*

7. K. Buet-Gautier, D. Soulat, J.L.Daniel, P.Boisse. 1999. "Simulations of Fiber Fabric Forming Accounting for Weaving", *Numisheet'99 13-17.*

8. P. Boisse, A. Cherouat, J.C. Gelin, and H. Sabhi.1995. "Experimental Study and Finite Element Simulation of a Glass Fiber Fabric and Shaping Process" *Polymer Composites, February 1995, Vol. 16, No. 1.*

9. T.M. McBride, J.Chen and L. Lam. "Effects of Formimg-Induced Evolution of Microstructure in Plain Weave Composites"

10. T.M. McBride and Julie Chen. 1997. "Unit-Cell Geometry in Plain-Waeve Fabrics During Shear Deformations" *Composites Science and Technology 57 (1997) 345-351.*

11. J. Ascough, H.E. Bez and A.M. Bricis. 1996. "A Simple Beam Element, Large Displacement Model for The Finite Element Simulation of Cloth Drape", *J. Text. Inst. 1996. 87 Part 1, No. 1.*

12. B.R. Mauget, L. Minetyan, and C.C. Chamis. "Large Deformation Nonlinear Response of Soft Composite Structures via Laminate Analogy"

13. P. Boisse, M.Borr, K. Buet and A. Cherouat. 1997. "Finite element simulations of textile composite forming including the biaxial fabric behaviour", *Composites Part B 28B (1997) 453-464.*

A. Hakim Cherouat and Jean Billoet. "Computational Simulation of The Shaping Process of Reinforced Composite Fabric By The Finite Element Method",1999. *Numisheet. 13-17.*

14. Yasser Gowayed and Li Yi, "Mechanical Behavior of textile composite materials using a Hybrid finite element approach". *Polymer Composite, Vol. 18, No.3. June*
15. *1997.*

16. D.M. Blackketter, D.E. Walrath and A.C. Hansen, "Modeling damage in a plain weave fabric reinforced composite material". *Journal of composites technology and research, JCTRER, Vol. 15, No. 2, Summer 1993, pp. 136-142*

17. John D. Whitcomb, "Three dimensional stress analysis of plain weave composite". *Composite Materials: Fatigue and fracture, third volume, 1991, pp.417-438*

18. Clinton Chapman and John Whitcomb, "Effect of assumed tow architecture on predicted moduli and stress in plain weave composite", *Journal of composite materials, Vol. 29. 1995*

19. G.E. Chadwick, S.A. Shorter and K Weissenberg. 1949. "A Trellis Model For The Application and Study of Simple Pulls in Textile Materials". *J of Text. Inst.,40, 108-160.*

20. Zhong Cai, Jenny Z. Yu, Frank K. Ko. "Formability of textile preforms for coomposite applications. Part 2: Evaluation experiments and modelling." Composites Manufacturing. Volume 5. Number 2. 1994.

21. Gommers, B., Verpoest, Van Houtte, P. "Determination of the Mechanical Properties of Composite Materials by Tensile Tests. Part 1: Elastic Properties." Journal of Composite Materials, Vol. 32, No. 4. 1998.

22. Simacek, Pavel, Advani, Suresh, G. " Permeability Model for Woven Fabric." Polymer Composites. Volume 17. No.6. 12/1996.

23. Piggott, M.R. " The Effect Of Fibre Waviness On The Mechanical Properties Of Unidirectional Fibre Composites" A Review. Composites Science and Technology. 53. 1995.

24. Masters, John, E., Minguet, Pierre, J. "Effect of Preform Architecture on Modulus and Strength of Two-Dimensional, Triaxially Braided, Textile Composite Materials." Composite Materials, Volume 12.

25. Zhong Cai, Jenny Z. Yu, Frank K. Ko. "Formability of textile preforms for coomposite applications. Part 2: Evaluation experiments and modelling." Composites Manufacturing. Volume 5. Number 2. 1994.

26. Gowayed, Yasser., Yi, Li. "Mechanical Behavioral of Textile Composites Materials Using a Hybrid Finite Element Approach." Polymer Composites. Volume 18. No. 3. 1997.

27. Wang, Y. Q., Wang, A.S.D. "On The Topological Yarn Structure of 3-D Rectangular And Tubular Braided Preforms." Composites Science and Technology. 51. 1994.